SINGLE-PHOTON OXIDATION OF C_{60} BY SELF-SENSITIZED SINGLET OXYGEN

By

LINQI ZHANG

Bachelor of Science in Mechanical Engineering
Harbin Institute of Technology
Harbin, Heilongjiang, China
2012

Master of Science in Mechanical and Aerospace Engineering
Oklahoma State University
Stillwater, Oklahoma
2014

Submitted to the Faculty of the
Graduate College of the
Oklahoma State University
in partial fulfillment of
the requirements for
the Degree of
DOCTOR OF PHILOSOPHY
December, 2020

SINGLE-PHOTON OXIDATION OF C_{60} BY SELF-SENSITIZED SINGLET OXYGEN

Dissertation Approved:

Dr. A. Kaan Kalkan

Dissertation Adviser

Dr. Sandip P. Harimkar

Dr. Shuodao Wang

Dr. Toby Nelson

ACKNOWLEDGMENTS

First and foremost, I would like to express my acknowledgment to my adviser, Dr. A. Kaan Kalkan, for his support, encouragement, warmhearted guidance and the exciting project he offered. Without his care, this dissertation would not have been possible.

I would also like to thank my dissertation committee Dr. Sandip P. Harimkar, Dr. Shuodao Wang and Dr. Toby Nelson for their valuable time and constructive feedback. I would like to extend my sincere thanks to Dr. Jacobs of Undergraduate Teaching Laboratory in the Chemistry Department for his training on Fluorolog Spectrometer, Dr. Steve Hartson in the OSU Genomics and Proteomics Center for his help in Mass Spectrometry and Dr. Jiming Bao in the University of Huston for his discussion in the singlet oxygen phosphorescence results.

My sincere thanks also go to Nishan and Karina of the Functional Nanomaterials Laboratory for their friendship.

Finally, I would like to thank my parents for their support and trust during my study.

Name: LINQI ZHANG

Date of Degree: DECEMBER, 2020

Title of Study: SINGLE-PHOTON OXIDATION OF C_{60} BY SELF-SENSITIZED SINGLET OXYGEN

Major Field: MECHANICAL AND AEROSPACE ENGINEERING

Abstract: Thanks to its unique properties, C_{60} has remarkably impacted nanoscience in the past two decades. Specifically, it is regarded as the most efficient singlet oxygen ($^1O_2$) photosensitizer. Yet, its oxidation by self-sensitized $^1O_2$ has not been known. The literature hints both oxygen and C_{60} must be at excited states to react, implying a 2-photon process: first, oxygen is photosensitized ($^1C_{60}\bullet{}^1O_2$); second, $^1C_{60}$* is photogenerated ($^1C_{60}*\bullet{}^1O_2$). However, this scheme is not plausible in a solvent, which would quench $^1O_2$ rapidly before the second photon is absorbed. Here, we uncover a single-photon oxidation mechanism via self-sensitized $^1O_2$ in solvents above an excitation energy of 3.7 eV. Using excitation spectroscopies and kinetics analysis, we deduce photoexcitation of a higher energy transient, $^3C_{60}**\bullet{}^3O_2$, converting to $^1C_{60}*\bullet{}^1O_2$. Such triplet-triplet annihilation, yielding two simultaneously excited singlets, is unique. It may empower other novel photochemistries with higher efficiency. Additionally, rate constants derived from this study allow us to predict a half-life of about a minute in the atmosphere, possibly explaining the scarceness of C_{60} in the environment.

TABLE OF CONTENTS

Chapter Page

I. INTRODUCTION 1
II. REVIEW OF LITERATURE 6
2.1. Molecular orbitals of C_{60} 6
2.2. Photophysical properties of C_{60} 8
2.3. Review of C_{60} photooxidation literature 10
2.4. Physical properties of $^1O_2$ 12
III. METHODOLOGY 14
3.1. C_{60} solution preparation 14
3.2. Theoretical calculation of O_2 to C_{60} ratio in solvents 14
3.3. Mass spectrometry 15
3.4. Photooxidation of C_{60} by UV and visible radiations 15
3.4.1. Exposure of C_{60} using a UV lamp 15
3.4.2. Exposure of C_{60} using LEDs 16
3.5. Estimation of the UV pumping rate of C_{60} 17
3.6. UV-Visible absorption spectroscopy 18
3.7. Fourier transform infrared spectroscopy 19
3.8. Phosphorescence spectroscopy 19
3.9. Excitation spectroscopy for phosphorescence 20
3.9.1. Excitation spectrum for $^1O_2$ phosphorescence 20
3.9.2. Excitation spectroscopy for photooxidation 20
IV. RESULTS AND DISCUSSION 22
4.1. Experimental results of C_{60} photooxidation 22
4.1.1. Mass spectrometry 22
4.1.2. UV-Visible spectroscopy 22
4.1.3. $^1O_2$ phosphorescence by Fluorolog-3 spectrofluorometer 25
4.1.4. Fourier transform infrared spectroscopy 26
4.2. Kinetics analysis of C_{60} photooxidation 27
4.2.1. Photooxidation kinetics of C_{60} in solvents 27
4.2.2. Extraction of k_{pd} from optical absorbance of C_{60} 28
4.2.3. Dependence of k_{pd} excitation intensity 29
4.3. Mechanism of C_{60} photooxidation 30
4.3.1. Proposal for C_{60} photooxidation schemes 30
4.3.2. Validation of the proposed photooxidation schemes 31
4.4. Mathematical model of oxidation kinetics 36
4.4.1. Oxidation of C_{60} with free $^1O_2$ 36
4.4.2. Oxidation of C_{60} with self-sensitized $^1O_2$ 39
4.5. Photooxidation of C_{60} in atmosphere 54

Chapter Page

4.5.1. Estimation of k_{pd} in the atmosphere under solar radiation..... 55
4.5.2. Half-life of C_{60} in the atmosphere 56
V. CONCLUSIONS..... 57
REFERENCES 60

LIST OF TABLES

Table Page

2.1. The lifetime of $^1\Delta_g$ oxygen in various solvents 13
4.1. IR mode assignments of C_{60} photoproducts after 6 h of photooxidation..... 27

LIST OF FIGURES

Figure Page

1.1. Schematic illustration of the "oxidation of C_{60} with self-sensitized $^1O_2$" model. First, a collision complex, $^1C_{60}\bullet{}^3O_2$ forms. Second, the $^1C_{60}$ is photoexcited to an excited singlet state ($^1C_{60}{}^{**}\bullet{}^3O_2$). Then the $^1C_{60}{}^{**}\bullet{}^3O_2$ converts to an excited triplet state ($^3C_{60}{}^{**}\bullet{}^3O_2$) via singlet-to-triplet conversion. Third, $^1O_2$ is photosensitized and C_{60} transitions to an excited singlet with lower energy ($^1C_{60}{}^{*}\bullet{}^1O_2$) simultaneously by triplet-triplet annihilation. Thereafter, both $^1C_{60}{}^{*}$ and $^1O_2$ are excited and readily to react. $C_{60}O$ is produced as the photoproduct. 4
2.1. π molecular orbitals of C_{60} 7
2.2. Absorption spectrum of C_{60} in hexane. Weak absorption in the visible range is shown in red in a smaller range of absorbance. 8
2.3. Energy structure of an isolated C_{60}. The pink curve represents the absorption spectrum of C_{60}. 9
2.4. Electronic configuration of the molecular oxygen. 12
3.1. Experimental setup for the radiation exposures of C_{60}. The UV lamp and 455 nm LED are shown. 16
3.2. Experimental setup for the radiation exposures of C_{60} with a 395 nm LED. 17
3.3. Phosphorescence (1270 nm) excitation spectra of C_{60} (in CCl_4) which were acquired in sequence. 21
4.1. Mass spectrum of the as-received C_{60} 23
4.2. Time series absorption spectra of C_{60} in C_6H_{14} (a), $CHCl_3$ (b) and CCl_4 (c) under UV excitation of 3.74 mW/cm^2. The inset of (c) shows photos of C_{60} solutions, unexposed and after 8 min of UV exposure. (d) The spectrum of the excitation source, UVP XX-15 UV lamp. 23
4.3. Absorption spectra of CCl_4 and C_{60} in CCl_4 at different concentrations. 24
4.4. Time series absorption spectra of C_{60} (in $CHCl_3$) under 395 nm excitation of 1 mW/cm^2 (a) and 455 nm excitation of 9 mW/cm^2 (b). 25
4.5. Phosphorescence spectra of $^1O_2$, sensitized by C_{60} (under 375 nm radiation of 9.5 mW/cm^2 intensity) in different solvents. 25
4.6. Phosphorescence spectra of $^1O_2$, sensitized by C_{60} (in CCl_4) under 395 (a) and 455 (b) nm radiation. 26
4.7. a) Time series FTIR spectra of C_{60} in $CHCl_3$ under the same UV exposure conditions as in Figure 4.2 (a-c). b) Assignment of FTIR peaks after 6 h of UV exposure (ρ: rocking; δ: bending; υ: stretching). 26
4.8. C_{60} time decay in different solvents. 27
4.9. Extraction of k_{pd} from $\frac{d}{dt}A(t,\lambda)$ for C_{60} in $CHCl_3$. 29

Figure Page

4.10. k_{pd} in CCl_4 as a function of irradiation intensity. 29
4.11. a) Overlay of absorption spectrum of C_{60} (black) and excitation spectrum for photosensitization of $^1O_2$ by C_{60}, monitored from $^1O_2$ phosphorescence counts at 1270 nm (red). b) Deconvolution of the phosphorescence excitation spectrum. 32
4.12. Overlay of normalized k_{pd} at different excitation wavelengths (black) and the deconvoluted 2^1H_u band (blue). Confidence interval error bars are shown (red) after 3 independent measurements. 34
4.13. Representative plots of $^1O_2$ phosphorescence intensity kinetics under continuous excitation of 310 nm (a) and 340 nm (b) wavelength. All 3 replications are shown. The plots are intentionally offset (separated) for clarity. 36
4.14. Mechanistic illustration of Scheme 3. 40
4.15. Fitting of theoretical k_{pd} expression to experimental data. The fitted values of k_{ox} and k_r are given in the inset. 50
4.16. Mechanistic illustration of Scheme 2. 51
4.17. Match of theoretical $^1O_2$ phosphorescence intensity (I) with experiment validating the k_q values adopted from the literature. k_{s2} (0.4 s^{-1}) is the sensitization rate by C_{60}. The 2 in the subscript indicates $h\nu$ < 3.7 eV. 54
4.18. a) AM 1.5 solar irradiation as a function of photon energy. b) The molar attenuation coefficient of C_{60} in hexane. The Gaussian fit, used in the numerical integration of ks, is shown in red. 56
5.1. Jablonski diagram illustrating single-photon oxidation of C_{60} with self-sensitized $^1O_2$. To a first approximation, we adopt the energy structure of isolated C_{60} for the C_{60} of C_{60}•O_2. The PO process involves the following steps: ① Excitation of C_{60} to C_{60}** by a single photon which has energy equal to or higher than 3.7 eV. ② Vibrational relaxation of C_{60}**. ③ Conversion of $^1C_{60}$** to $^3C_{60}$** by ISC. ④ Sensitization of $^1O_2$ from $^3O_2$ by $^3C_{60}$** via TTA. Partial energy of $^3C_{60}$** is utilized in the $^1O_2$ sensitization, and the $^3C_{60}$** falls to a lower electronically excited state ($^1C_{60}$*). ⑤ Production of $C_{60}O$ by reaction of $^1C_{60}$* with $^1O_2$. 58

CHAPTER I

INTRODUCTION

Buckminsterfullerene (C_{60}), or the "bucky ball", was discovered by Kroto *et al.*[1] in 1985. It is the most famous member of the fullerene family. The words "fullerene" and "bucky ball" are after the American architect Buckminster Fuller, because the structure of C_{60} and other fullerenes looks like one of his famous architectural designs, the geodesic dome. C_{60} is the most symmetric form of carbon ever known. Kroto *et al.* were also awarded the Nobel Prize, owing to their discovery of this unique carbon structure. In 1990, Krätschmer *et al.*[2] developed a method to produce macroscopic quantities of C_{60} by evaporating graphite electrodes in helium (100 Torr). Their work is phenomenal because it allows a sufficient amount of C_{60} to be produced for instrumental characterization, therefore stimulating a whole range of research on C_{60}. Since then, many unique and outstanding properties of C_{60} have been found.

C_{60} is a good electron acceptor. It has the ability of accepting up to six electrons. Due to this strong electron attracting ability, C_{60} has been functionalized by numerous compounds (e.g., C_{60} derivatives) to reach desired properties. The optoelectronic properties of C_{60} (as well as the C_{60} derivatives) have inspired applications in photovoltaics,[3] photocatalysis[4], and molecular probes.[5] Additionally, C_{60} is the most efficient singlet oxygen ($^1O_2$) sensitizer ever known, due to its high intersystem crossing quantum yield (allowed by the high symmetry of C_{60}) and long-lived triplet states. This fascinating property has been facilitating the medical research in photodynamic therapy,[6,7] where $^1O_2$ is photosensitized by C_{60} to kill cancer cells or pathogens. Similarly, a

thriving research endeavor is to exploit $^1O_2$ in environmental cleanup,[8] such as water disinfection and plastic waste degradation. Altogether, C_{60} has not only made a remarkable impact in science and technology formerly but will also continue to be instrumental in newly emerging research fronts.

Even though C_{60} has many unique properties and promising applications, a major concern is photodegradation of C_{60} in these applications, which however has not been meticulously investigated. C_{60} is found to be unstable under solar radiation in the air. Initial work on photooxidation (PO) of C_{60} credited it to ozonation,[9–11] which however is limited to excitation wavelengths shorter than 240 nm for photogeneration of O_3.[12] On the contrary, PO of C_{60} by self-sensitized $^1O_2$ is more probable and was proposed in the literature.[13–15] To this end, the most seminal findings have been: i) C_{60} does not react with externally-produced $^1O_2$ unless it is photoexcited;[14] ii) PO can occur under ultra-violet (UV) excitation (308 nm) in O_2 ambient (albeit formation of $^1O_2$ did not collaborate);[15] and iii) $C_{60}O$ is the major photoproduct.[14–16] However, the mechanistic details of the photophysics and photochemistry remain unelucidated. Typically, a photochemist would propose a two-photon process for the PO, where the first photon is used to sensitize $^1O_2$ and the second one excites C_{60}. While this picture is valid in the air, where $^1O_2$ lifetime is for minutes, it is not plausible in solvents, where $^1O_2$ lifetime is much shorter. $^1O_2$ would rapidly be quenched by solvents before the second photon is absorbed.

The present dissertation work demonstrates the PO of C_{60} by self-sensitized $^1O_2$ via a single-photon above 3.7 eV in solvents, using kinetics analysis and excitation spectroscopies. The kinetics study was performed by photoexcitation of C_{60} in solvents with different $^1O_2$ lifetimes (τ). One major finding from the kinetics analysis is the dependence of C_{60} photodecay rate (k_{pd}) on τ, which has not been reported anywhere in the literature. In addition, the kinetics analysis also shows an exponential decay of C_{60} and a linear dependence of k_{pd} on radiation intensity.

Therefore, for the first time in the literature, we demonstrate PO of C_{60} can be a single-photon process.

To validate/elucidate this mechanism of C_{60} PO, we first developed a model, named "oxidation of C_{60} with free $^1O_2$". In this model, $^1O_2$ is released to the solvent after photosensitized by a C_{60}. Subsequently, it collides and reacts with an excited singlet C_{60} unless quenched by the solvent. This model consistent with our observation that k_{pd} increases with τ. However, our calculation (on the optical pumping rate of C_{60}) shows the excited singlet C_{60} and $^1O_2$ will hardly coincide in time, due to a fast quenching of $^1O_2$ by solvents. Therefore, the PO of C_{60} will not happen. Additionally, PO of C_{60} described by this model is a two-photon process, which disagrees with our kinetics result. Therefore, the "oxidation of C_{60} with free $^1O_2$" model is ruled out.

Instead, we propose "oxidation of C_{60} with self-sensitized $^1O_2$" model where excitation of O_2 and C_{60} occurs simultaneously via a single-photon. In this model, the single-photon energy is partially utilized in sensitizing $^1O_2$ while the excess energy leaves C_{60} at an excited state, which can react with $^1O_2$. A schematic illustration of this model is shown in Figure 1.1. Corroborating with the energy diagram of C_{60}, we find the single-photon needs minimum excitation energy of 3.7 eV, being remarkably close to the energy threshold of $^1A_g \rightarrow 2^1H_u$ transition (3.72 eV in literature).[17] Experimentally, k_{pd}s at different excitation wavelengths were derived in this work. We found that k_{pd} increases significantly at a threshold of excitation energy at 3.7 eV. Additionally, the k_{pd}s at different excitation wavelengths show a Gaussian distribution, which matches the $^1A_g \rightarrow 2^1H_u$ Gaussian band deconvoluted from the excitation spectrum of C_{60} for $^1O_2$ phosphorescence. Those findings suggest PO of C_{60} is driven by the $^1A_g \rightarrow 2^1H_u$ transition with a photon energy threshold of 3.7 eV.

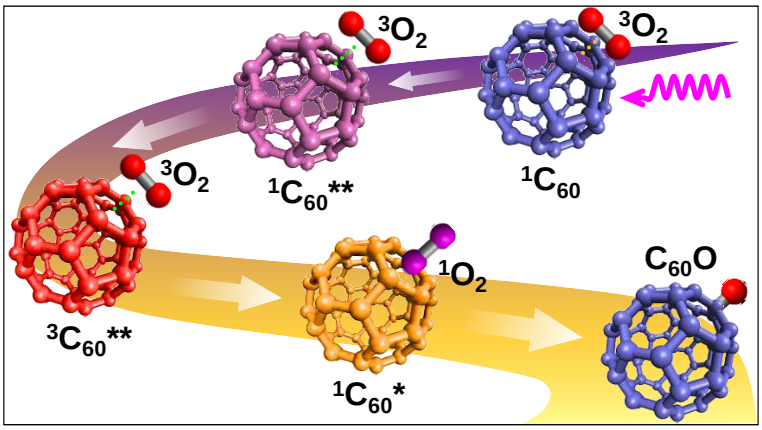

Figure 1.1: Schematic illustration of the "oxidation of C_{60} with self-sensitized $^1O_2$" model. First, a collision complex, $^1C_{60}\bullet{}^3O_2$ forms. Second, the $^1C_{60}$ is photoexcited to an excited singlet state ($^1C_{60}$**$\bullet{}^3O_2$). Then the $^1C_{60}$**$\bullet{}^3O_2$ converts to an excited triplet state ($^3C_{60}$**$\bullet{}^3O_2$) via singlet-to-triplet conversion. Third, $^1O_2$ is photosensitized and C_{60} transitions to an excited singlet with lower energy ($^1C_{60}$*$\bullet{}^1O_2$) simultaneously by triplet-triplet annihilation. Thereafter, both $^1C_{60}$* and $^1O_2$ are excited and readily to react. $C_{60}O$ is produced as the photoproduct.

A major attribute of the present dissertation is the discovery of a unique triplet-triplet annihilation (TTA) process during C_{60} PO. By its description in the literature, TTA involves Dexter energy transfer from a triplet to another, after which the acceptor transitions to a higher energy state, while the donor returns to its ground singlet state. However, in our work, two simultaneously-excited singlets ($^1C_{60}$* and $^1O_2$) are produced by TTA as shown in Figure 1.1. This new TTA, yielding two simultaneously-excited singlets, was never reported in the literature and it may enable other novel photochemistries with high efficiency.

Finally, we predict PO of C_{60} in the atmosphere dominantly occur as a two-photon process driven by visible and UVA photons, being abundant in solar radiation. Different from solvents, the τ in the air is dramatically prolonged, therefore a 2-photon oxidation is plausible. Though, it is challenging to monitor the PO of C_{60} suspended in a gas, such as air, due to its aggregation as well as adsorption to enclosure walls at measurable concentrations. To this end, our work is critical, because we are able to compute the k_{pd} of C_{60} in the atmosphere using the rate constants (e.g., k_{ox} ('ox' for oxidation) and k_r ('r' for relaxation)) captured in our work (i.e., C_{60} in

solvents). Those rate constants are the intrinsic property of C_{60}, which remains the same despite the change in surroundings. Accordingly, we predict a C_{60} half-life of about a minute in the atmosphere, possibly explaining the scarceness of C_{60} in the environment.

The organization of the present dissertation is as follows. Chapter 2 reviews the physical properties of C_{60} and $^1O_2$. A historical review of the C_{60} PO literature is also provided. In Chapter 3, experimental procedures on the characterization of C_{60} PO are detailed. Chapter 4 presents the experimental results. The PO kinetics was monitored by UV-Visible spectroscopy. Fourier transform infrared (FTIR) spectroscopy is used to corroborate the oxidation of C_{60}. Excitation and phosphorescence spectroscopies are performed to reveal the PO mechanism. The mechanism is also corroborated with two mathematical models developed in this work. PO of C_{60} in the atmosphere is also predicted. Finally, various conclusions are drawn in Chapter 5.

CHAPTER II

REVIEW OF LITERATURE

2.1. Molecular orbitals of C_{60}

C_{60} is the roundest and most symmetrical molecule known in the literature. It is composed of 12 pentagons and 20 hexagons of carbon atoms, connecting together to form a spherical shape, resembling a traditional soccer ball. Each carbon atom contributes 4 electrons in C_{60} molecular orbitals (MOs). Hence, C_{60} contains 240 MOs (120 occupied and 120 unoccupied) in total. To a first approximation (sp^2 hybridization), each carbon is bonded to three others via 3 σ bonds and 1 π bond. Therefore, among the 240 MOs, 60 MOs (30 occupied (bonding) and 30 unoccupied (antibonding)) are π type and 180 are σ type. However, the actual bonding between carbons is strongly restricted by the spherical geometry of C_{60}. Haddon *et al.*[18] indicate the real hybridization of carbon is $sp^{2.3}$. But, for the sake of simplicity, the first approximation is still widely assumed in the literature.[19] To the first approximation, the 60 π electrons are considered to be delocalized over the surface of C_{60}. Therefore, one can find the π MOs of C_{60} by solving the spherical harmonics of Schrödinger's equation for a particle on a sphere. On the other hand, one should also know that C_{60} is a truncated icosahedron (e.g., I_h symmetry) rather than a perfect sphere in reality. As a result, few higher energy orbitals determined by the spherical symmetry split under icosahedral symmetry. The splitting of MOs of C_{60}, as well as the corresponding orbital symmetry (e.g., gerade or ungerade), are shown in Figure 2.1.[18,20,21]

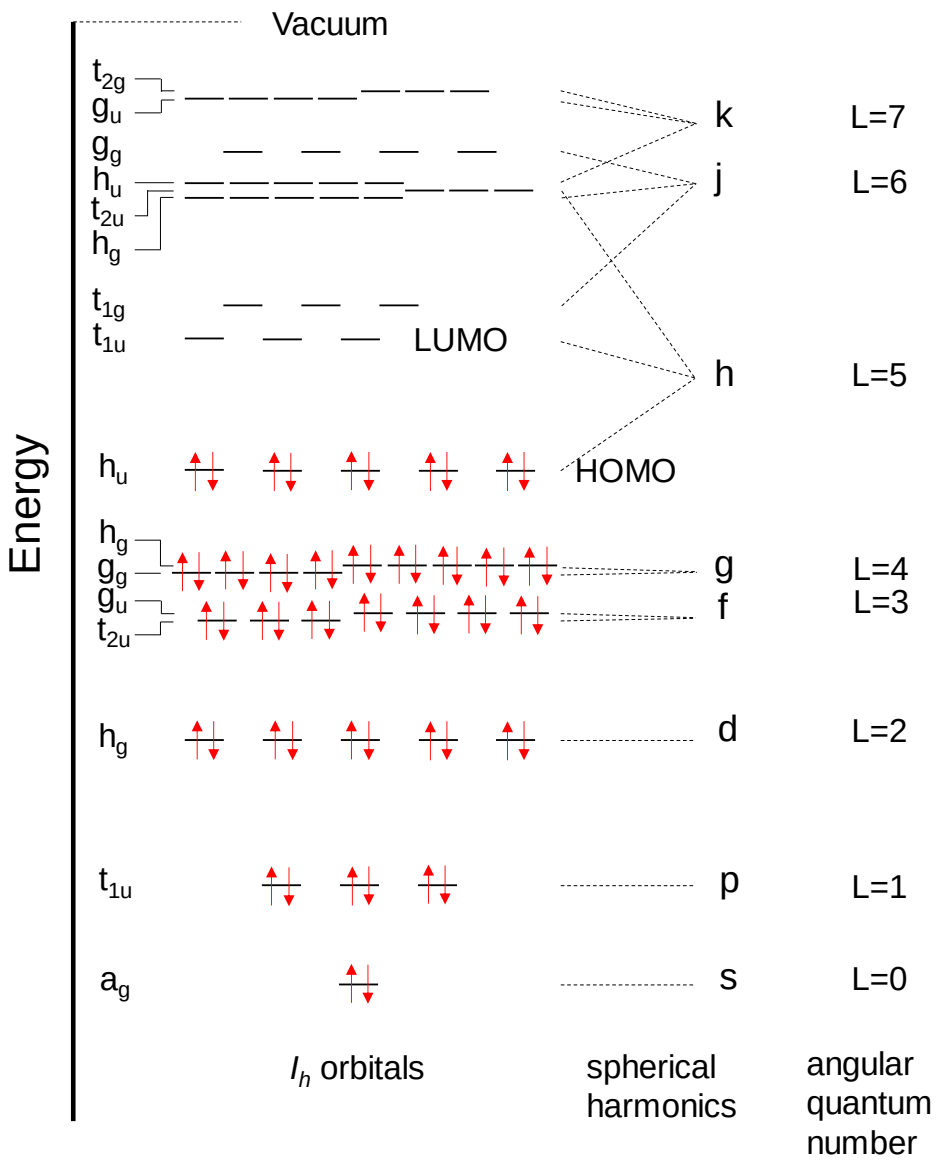

Figure 2.1: π molecular orbitals of C_{60}.

The energies of the highest occupied molecular orbital (HOMO) and the lowest unoccupied molecular orbital (LUMO) of C_{60} are found to be –6.1 and –4.3 eV versus the vacuum,[21] respectively, resulting in a bandgap of 1.8 eV. However, we need to point out that the bandgap, as well as the MO energy of C_{60}, remain debatable in the literature and various bandgap values were reported.[22–25] After placing 60 π electrons in the MOs in Figure 2.1, the following properties are suggested: 1) C_{60} is a diamagnetic molecule because all electrons are paired; 2) C_{60}

is a good electron acceptor, given its low-lying unoccupied energy level with room for 6 electrons; 3) The HOMO to LUMO transition is forbidden due to the orbital symmetry.

2.2. Photophysical properties of C_{60}

The ground state of C_{60} is a singlet state (e.g., 1^1A_g) given all electron spins are paired. The lowest four excited states of C_{60} are 1^1T_{2g}, 1^1T_{1g}, 1^1G_g, and 1^1H_g states, which have the same symmetry as the ground state. Therefore, transitions from the ground state to those excited states are forbidden (e.g., HOMO to LUMO transition of C_{60} is forbidden as shown in Figure 2.1). As a result, C_{60} presents a very weak absorption in the visible range (from 430 to 640 nm) as shown in Figure 2.2. The absorption of C_{60} in the visible range is credited to vibronic interactions.[26] On the other hand, C_{60} absorbs strongly in ultraviolet (UV) radiation. Three major absorption peaks at 209, 256 and 328 nm are shown in Figure 2.2, which correspond to the allowed transitions from the grand state to higher excited states. A comprehensive energy structure of an isolated C_{60} is shown in Figure 2.3.[17]

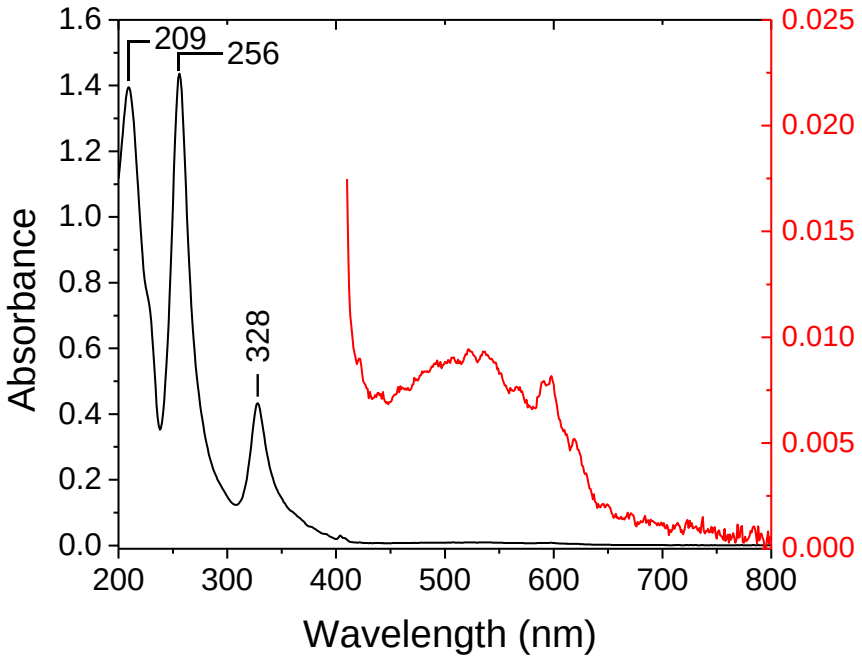

Figure 2.2: Absorption spectrum of C_{60} in hexane. Weak absorption in the visible range is shown in red in a smaller range of absorbance.

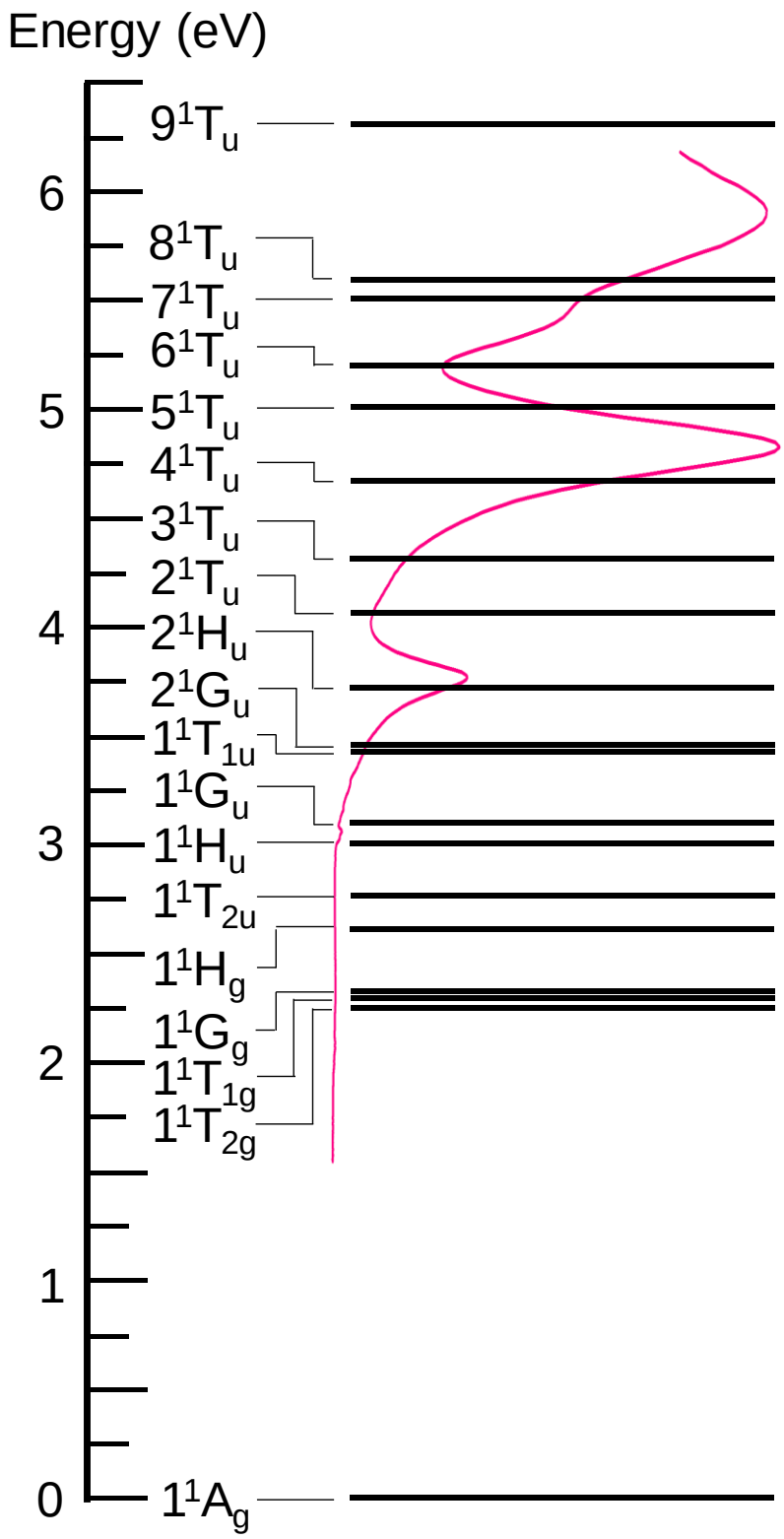

Figure 2.3: Energy structure of an isolated C_{60}. The pink curve represents the absorption spectrum of C_{60}.

Transitions from the lowest four excited states to the ground state of C_{60} are also symmetry forbidden. This is partially responsible for the weak fluorescence emission of C_{60}. A second reason for the weak fluorescence emission is the efficient singlet-to-triplet conversion ($1^1T_{1g} \rightarrow 1^3T_{1g}$) due to a large spin-orbital coupling in C_{60}.[27] This effective conversion leads to a short excited singlet lifetime of C_{60} (1.2 ns). On the contrary, the excited triplet lifetime of C_{60} is long (40 μs),[28] because the transition from excited triplet state to the ground state of C_{60} is spin forbidden. This long triplet lifetime allows C_{60} to efficiently sensitize a molecule at its triplet state, such as $^3O_2$. C_{60} is the most efficient $^1O_2$ photosensitizer even known. Foote *et al.*[28] and others[29,30] have shown the quantum yield of $^1O_2$ sensitization is close to unity for excitation of C_{60} in the visible. Foote[26] has also reported no phosphorescence is detectable for C_{60}.

2.3. Review of C_{60} photooxidation literature

Photooxidation (PO) of C_{60} was first observed by Taylor *et al.*[11] They found undissolved reddish-brown deposit after exposing their freshly prepared C_{60} in benzene (open to air) to UV radiation (using a water-cooled medium-pressure silica-jacketed Hanovia insertion UV lamp). They also observed extensive oxidation of C_{60} after 10-16 h of UV exposure. They credited this PO to oxidation by O_3 (e.g., ozonation of C_{60}). A year later, Creegan *et al.* photooxidized C_{60} in benzene and found C_{60} epoxide ($C_{60}O$) as the primary photoproduct.[16] Heymann *et al.* also claimed ozonation of C_{60}. They detected $C_{60}O$ as well as other C_{60}-adducts (i.e., $C_{60}O_2$, $C_{60}O_3$) when C_{60} was exposed to O_3 in toluene.[9] Seven years later, they identified fullerene ozonide (e.g., $C_{60}O_3$) as the reaction intermediate in the C_{60} oxidation reaction. They reported C_{60} first reacted with an O_3 molecule and produced $C_{60}O_3$. Subsequently, $C_{60}O_3$ dissociated to a $C_{60}O$ and an O_2 molecule.[31] Ozonation of C_{60} in the ambient atmosphere (traceable amount of ozone) and ozone-enriched water was later reported by Murdianti *et al.*[32] and Fortner *et al.*,[33] respectively.

An alternative mechanism for C_{60} PO is the oxidation of C_{60} by $^1O_2$. Foote *et al.* found the $^1O_2$ sensitization quantum yield of C_{60} to be 0.96 ± 0.04 at 532 nm laser excitation, but 0.76 ± 0.05 at 355 nm excitation.[28] However, they could not provide an explanation for the lower sensitization yield at 355 nm. The same year, Wood *et al.*[34] also observed the degradation of C_{60} in benzene under UV radiation (using a 150 W mercury arc lamp) and found $C_{60}O_n$ (n=1 to 5) as photoproducts by mass spectrometry. Later, in 1993, Taliani *et al.*[13] reported the detection of $C_{60}O_2$ after exposing a C_{60} film (5 μm thick) to an Ar^+ laser (λ=488 nm). To explain the formation of the photoproducts, they proposed the mechanism of $^1O_2$ addition to C═C in the C_{60} cage. However, this explanation has not been corroborated in terms of the photoproducts reported in the literature on the photoproducts.[14–16,34,35]

In the same year, Juha *et al.*[36] reported a fast decomposition of C_{60} when radiated in hexane with a XeCl-excimer laser (308 nm). A year later, they identified the photoproduct to be $C_{60}O$ by liquid chromatography.[15] In addition, they observed no reaction between ground state C_{60} with externally generated $^1O_2$ stream. Accordingly, they concluded C_{60} needed to be electronically excited in order to react with $^1O_2$. Given C_{60} is an excellent $^1O_2$ photosensitizer, it is reasonable to anticipate $^1O_2$ was photosensitized by C_{60} in Juha's work by laser excitation. However, no direct evidence was provided to this end.

Finally, a more compelling elucidation was contributed by Schuster *et al.*[14] They excited C_{60} by a Hanovia 450 W medium pressure Hg arc lamp (200-400 nm) in a $^1O_2$ environment (produced by thermolysis of endoperoxides) and found a large yield of $C_{60}O$. In contrast, significantly lower yield of $C_{60}O$ was observed in the absence of $^1O_2$. This finding confirms the role of $^1O_2$ plays in C_{60} oxidation, but the mechanistic details of the reaction remain unknown. Schuster *et al.* have proposed the mechanism of $C_{60}O$ formation to be the reaction of $^1O_2$ with the triplet state of C_{60}. However, this explanation is not plausible because the proposed reaction is spin forbidden.

2.4. Physical properties of $^1O_2$

Singlet oxygen was first proposed by Mulliken *et al.* in 1928.[37] Unlike C_{60} and most molecules, the ground state of oxygen ($^3\Sigma_g^-$) is a spin-triplet. However, oxygen molecules have two low-lying excited electronic states, $^1\Delta_g$ and $^1\Sigma_g^+$, both of which are spin singlets.[38] The $^1\Delta_g$ and $^1\Sigma_g^+$ states have 22.4 and 37.8 kcal/mol higher energy than the $^3\Sigma_g^-$ state.[39] The $^3\Sigma_g^-$ and $^1\Sigma_g^+$ oxygen have identical electronic configuration, but the two electrons in π^* orbits have different spins. The electronic structure of the $^1O_2$ is shown in Figure. 2.4.

The $^1\Delta_g$ oxygen is a relatively long-lived oxidant species (lifetime of $^1\Delta_g$ oxygen is 45 min in the atmosphere)[40] due to its spin-forbidden transition from the $^1\Delta_g$ state to the $^3\Sigma_g^-$ state. However, the lifetime of $^1\Delta_g$ oxygen drops significantly in solvents, mainly due to the energy quenching by C─H and O─H bond vibrations.[38] The lifetime of $^1\Delta_g$ oxygen in various solvents is listed in Table 2.1.[41] On the other hand, $^1\Sigma_g^+$ oxygen is a short-lived oxidant species because of a spin-allowed transition to the $^1\Delta_g$ state.[40] The transition from the $^1\Delta_g$ state to the $^3\Sigma_g^-$ state results in light emission (phosphorescence) at 1270 nm. This intrinsic property is applied for the detection of $^1O_2$, which was first suggested by Khan *et al.*[42]

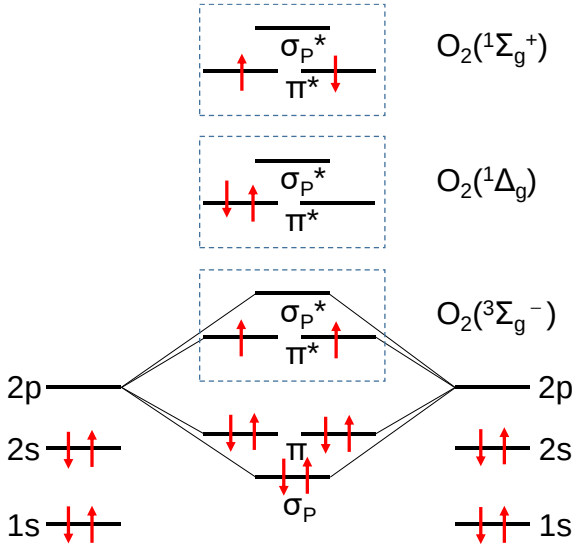

Figure 2.4: Electronic configuration of the molecular oxygen.

Table 2.1. The lifetime of $^1\Delta_g$ oxygen in various solvents

Solvent	τ(μs)	Solvent	τ(μs)
Toluene	29	Benzene	31
Acetone	51	Acetonitrile	75
Diethyl ether	34	Chloroform	207
Pyridine	16	Carbon disulfide	34000
Dioxane	27	Carbon tetrachloride	87000
Hexafluorobenzene	3900	Freon-113	99000
Chlorobenzene	45	Water	~5
Hexane	30	methanol	10.4

CHAPTER III

METHODOLOGY

3.1. C_{60} solution preparation

A stock solution of C_{60} was first prepared by dissolving 1 mg of C_{60} (Thermo Fisher Scientific, >99.9%) in 10 ml of solvent via ultra-sonication for 30 min. Next, the solution was kept undisturbed in the dark for 30 min to let insoluble aggregates (e.g., $C_{60}O$) settle down. Subsequently, the supernatant was transferred by a pipette to a spectrophotometer cell (optical path length of 10 mm) filled with the same solvent until the absorbance of C_{60} at 256 nm reaches ~1.42 (as monitored by a spectrophotometer), corresponding to C_{60} concentration of 5.67 μM. Finally, the prepared solution was stored in a sealed glass vail and kept in dark before use. High purity of C_{60} in the prepared C_{60} solution (e.g., in Chloroform ($CHCl_3$)) is confirmed by Mass Spectrometry (Section 3.3). C_{60} in Hexane (C_6H_{14}), $CHCl_3$ and Carbon Tetrachloride (CCl_4) are prepared in this work. The C_6H_{14} and $CHCl_3$were purchased from the Chemistry Store of Oklahoma State University. The CCl_4 (HPLC grade, 99.9+%) was purchased from Sigma Aldrich. All solvents were used without further purification.

3.2. Theoretical calculation of O_2 to C_{60} ratio in solvents

The mole fraction solubility of a gas in a solvent, x_g, is defined as[43]

$$x_g = \frac{n_g}{n_g + n_s} \tag{3.1}$$

where n_g is the maximum number of moles of the gas soluble in n_s moles of the solvent.

x_g of O_2 in C_6H_{14}, $CHCl_3$ and CCl_4 are given as 2.26×10^{-3}, 0.73×10^{-3} and 1×10^{-3} in the literature.[43–45] Taking 1 L of the solvent, we compute n_s using the density and molar mass of the solvent from the literature. Then, n_g is computed from Equation 3.1 which also equals the molar concentration of the gas. Accordingly, the O_2 concentration in C_6H_{14}, $CHCl_3$, and CCl_4 are calculated as 1.72×10^{-2}, 9.12×10^{-3} and 1.03×10^{-2} M, respectively. The default C_{60} concentration is 5.67 μM in all solvents (Section 3.1). Hence, the O_2 to C_{60} ratio in C_6H_{14}, $CHCl_3$, and CCl_4 are computed as 3034:1, 1608:1 and 1817:1, respectively.

3.3. Mass spectrometry

The purity of C_{60} in solution before UV exposure (as-received C_{60}) is checked by an LTQ-OrbitrapXL mass spectrometer (Thermo Fisher Scientific). Specifically, 250 μL of C_{60} solution (in $CHCl_3$) was infused into an electrospray chamber by a syringe pump at a flow rate of 30 μL/min. The MS spectrum was collected at the negative ion mode with a negative ion spray voltage of 3500 V and ion transfer tube temperature of 300 ℃. Nitrogen drying gas at 80 ℃ was supplied to evaporate the solvent. The scan range was set from 700 to 820 m/z and the maximum injection time was set to 100 ms.

3.4. Photooxidation of C_{60} by UV and visible radiations

3.4.1. Exposure of C_{60} using a UV lamp

In this process, 4 ml of C_{60} solution (prepared as described in Section 3.1) was transferred to a quartz optical cell (Starna Cells, 10 mm optical length, 4 ml capacity). Subsequently, the cell was sealed with a plastic cap using Parafilm. Then, the cell was placed on an adjustable stage and exposed to UV radiation at 3.74 mW/cm^2 as shown in Figure 3.1. The radiation (spectrum centered at 310 nm) was generated by a pair of tube lamps (Ultra-Violet Products, XX-15 series, 15 W each) and the UV intensity was measured by a digital UVA/UVB meter (General Tools UV513AB).

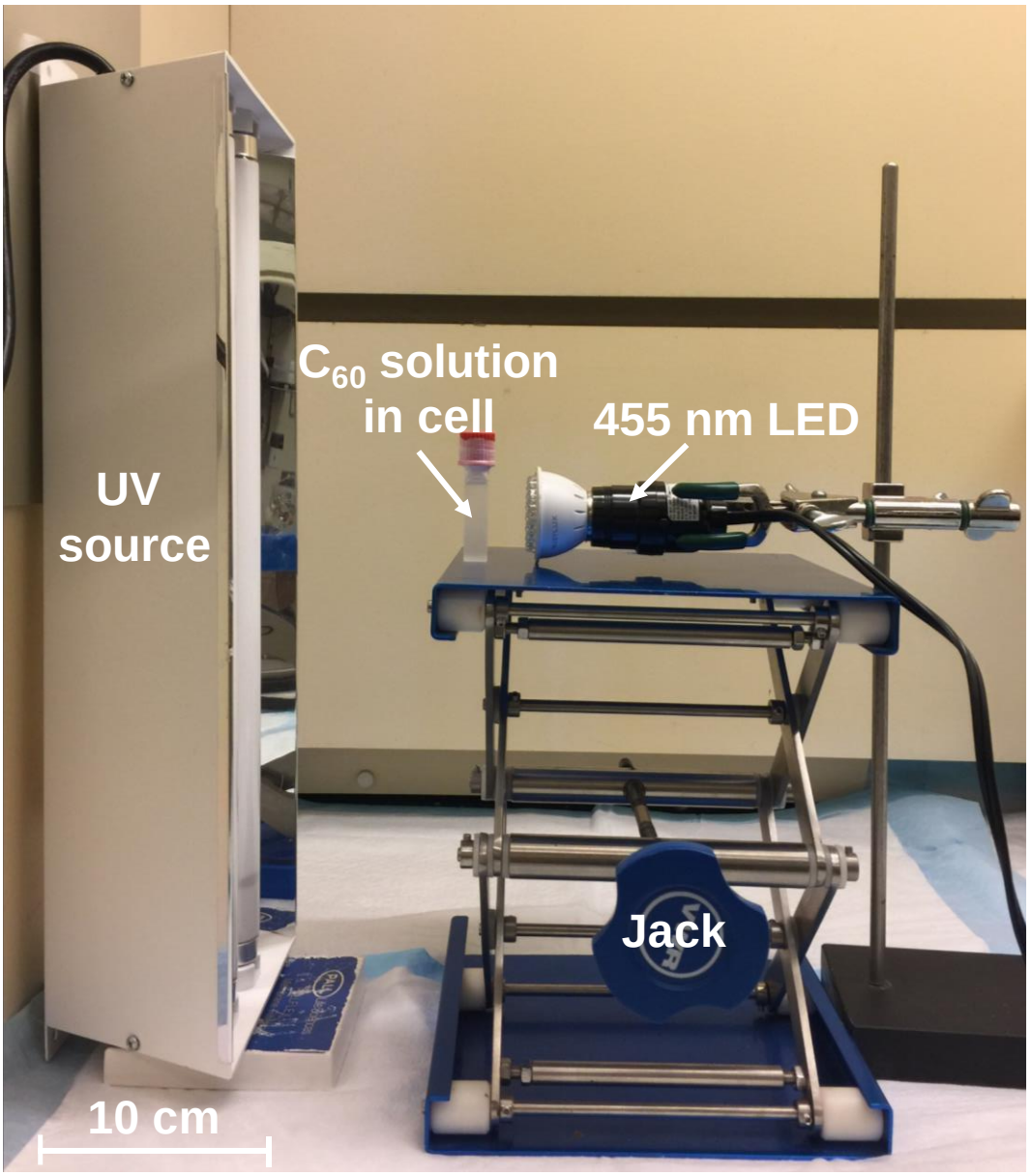

Figure 3.1: Experimental setup for the radiation exposures of C_{60}. The UV lamp and 455 nm LED are shown.

3.4.2. Exposure of C_{60} using LEDs

C_{60} in $CHCl_3$ (as described in Section 3.4.1) was exposed to LEDs at wavelengths of 455 and 395 nm. The 455 nm radiation (9 mW/cm^2) was provided by an LED bulb (RubyLux) as shown in Figure 3.1. The 395 nm radiation (1 mW/cm^2) was provided by a replaceable LED coupled to an SL1-LED light source (StellarNet) as shown in Figure 3.2. The intensity was measured by a compact USB power meter (Thorlabs, PM16-121).

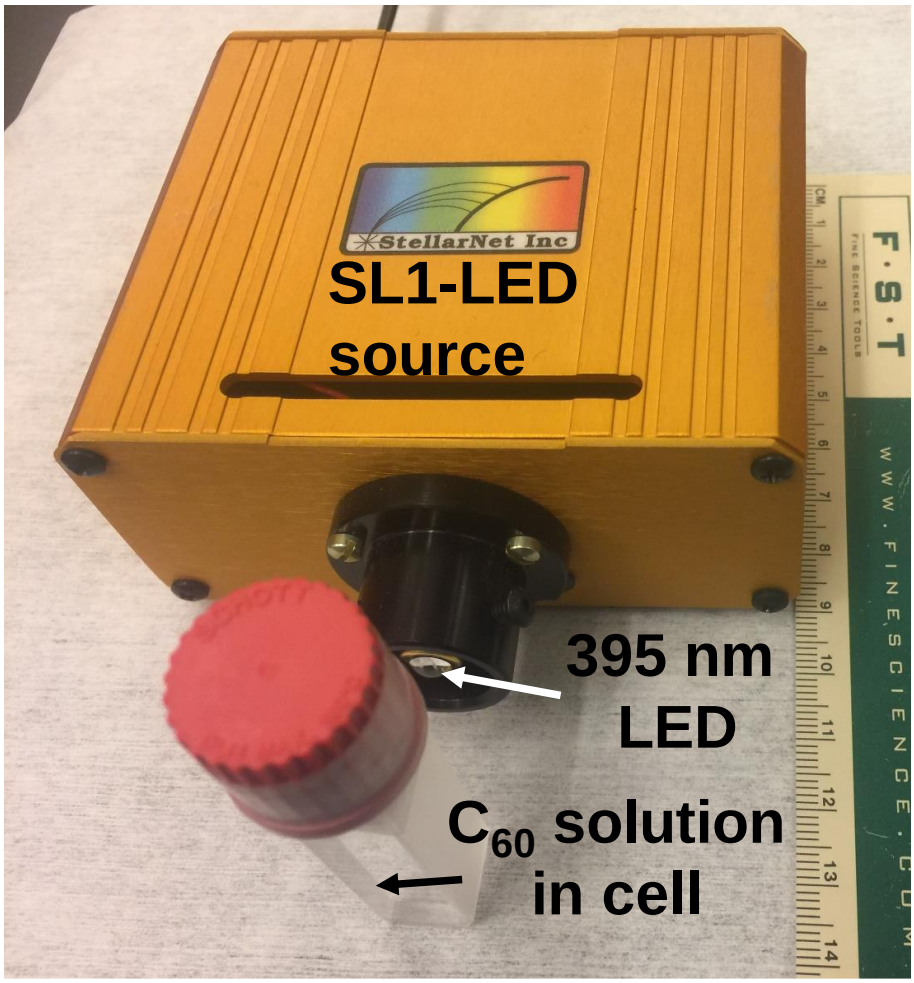

Figure 3.2: Experimental setup for the radiation exposures of C_{60} with a 395 nm LED.

3.5. Estimation of the UV pumping rate of C_{60}

Here, we are estimating the transition (optical pumping) rate for ${}^1A_g \longrightarrow 2\ {}^1H_u$ under UV radiation (as described in Section 3.4.1). From Figure 2.3, the $2\ {}^1H_u$ of C_{60} has an energy of 3.72 eV, which is right below the UV excitation energy (i.e., 4 eV) used in this work. The pumping rate, k_p, can be derived from:

$$P(\upsilon) = \sigma_{abs}(\upsilon) \cdot I(\upsilon) = k_p(\upsilon) \cdot h\upsilon \tag{3.2}$$

where P is the power absorbed by a single C_{60} molecule, σ_{abs} is its absorption cross-section, I is the radiation intensity, and $h\upsilon$ is the photon energy. We will also use the relationship between the absorption cross-section and molar attenuation coefficient, ε, as:

$$\sigma_{abs} = 3.8\times10^{-21}\varepsilon\ (\sigma_{abs}\ in\ cm^2\ and\ \varepsilon\ in\ M^{-1}cm^{-1}) \tag{3.3}$$

Hence,

$$k_p(\upsilon) = \frac{3.8\times10^{-21}\varepsilon(\upsilon)\cdot I(\upsilon)}{h\upsilon} \tag{3.4}$$

For the exact computation of k_p, Equation 3.4 should be integrated over the energy range of the ${}^1A_g \longrightarrow 2\ {}^1H_u$ transition, I being per photon energy. However, resolving ε for ${}^1A_g \longrightarrow 2\ {}^1H_u$ is difficult as it overlaps with multiple and higher oscillator strength transitions. Here, we need a conservative estimate of k_p for validating various assumptions and approximations in Section 4.4. As will be discussed in Section 4.4, a sufficiently low value of k_p is needed. Therefore, for a conservative approximation, we adopt an overestimated average value of ε and simplify the integration to a multiplication (Equation 3.4), using the integrated value of I, $I = 3.74\ mW/cm^2$. Accordingly, we pick ε of C_{60} at $h\upsilon = 4.0\ eV$ ($\varepsilon = 1.2\times10^4\ M^{-1}cm^{-1}$).[46] This value of ε is conservative (overestimated), because photon energy of $h\upsilon = 4.0\ eV$ ($\lambda = 310\ nm$) is close to the center (maximum) of the ${}^1A_g \longrightarrow 2\ {}^1H_u$ absorption band (i.e., $\lambda = 299\ nm$, will be shown in Figure 4.10b). Furthermore, additional transitions contribute to ε at $h\upsilon = 4.0\ eV$. Accordingly, k_p is computed as $0.27\ s^{-1}$.

3.6. UV-Visible absorption spectroscopy

The absorption spectra of C_{60} were acquired with a Varian Cary 300 double-beam UV-Vis spectrophotometer. The spectra were measured before and during UV exposures (i.e., after each exposure interval) during photooxidation. The pure solvent was used as the reference. The

spectra were recorded in the wavelength range from 200 to 800 nm with data intervals of 1 nm. The scan rate was set to 600 nm/min.

3.7. Fourier transform infrared spectroscopy

A Bruker Alpha FTIR spectrometer, operating in the attenuated total reflection (ATR) mode was employed. In a typical acquisition, 10 µl of C_{60} solution (in $CHCl_3$) was spotted on the ATR diamond detector. However, for higher signal-to-noise, the spectrum of C_{60} after 6 h exposure was measured after casting 50 µl of C_{60} solution on the detector. Spectra were acquired after complete evaporation of the solvent at a resolution of 4 cm^{-1} and 24 scans-to-average in the wavenumber range of 500-3500 cm^{-1}.

3.8. Phosphorescence spectroscopy

The $^1O_2$ phosphorescence spectra in solvents (i.e., C_6H_{14}, $CHCl_3$, and CCl_4) were acquired by Fluorolog-3 spectrofluorometer (Horiba Jobin Yvon) equipped with an LN2-cooled solid-state IR detector (DDS-Series) and a xenon lamp (450 W) as the excitation source. In a typical acquisition, 200 µl of C_{60} solution was placed in a standard micro fluorescence cuvette (Science Outlet, 10 mm optical length, 0.7 ml capacity). Pure solution spectrum was used as the baseline. The Fluorolog system automatically normalizes the signal intensity by the source (i.e., the xenon lamp) intensity, which is measured by the reference detector. The excitation wavelength was parked at 375 nm with a bandpass of 5 nm. The incident power was measured as 1.9 mW with a power meter (Thorlabs, PM16-121). The emission was scanned from 1225 to 1325 nm using bandpass of 20 nm. The data interval was set to 1 nm. The signal was integrated for 15 s per data point for C_{60} in C_6H_{14} and $CHCl_3$ and 3s per data point for C_{60} in CCl_4.

Additionally, the $^1O_2$ phosphorescence spectra of C_{60} in CCl_4 at excitation wavelengths of 395 and 455 nm were also acquired in this work. Following parameters are applied: excitation

bandpass of 5 nm, emission bandpass of 20 nm, data interval of 1 nm, and detector integration time of 4 s.

3.9. Excitation spectroscopy for phosphorescence

3.9.1. Excitation spectrum for $^1O_2$ phosphorescence

The excitation spectrum of C_{60} for $^1O_2$ phosphorescence ($^1O_2$ photosensitization) was acquired by Fluorolog-3 spectrofluorometer. C_{60} dissolved in CCl_4 and pure CCl_4 were used as the sample (signal) and baseline, respectively. The sample and baseline liquids were enclosed in a quartz cuvette (Science Outlet, 10 mm optical length, 4 ml capacity) during the acquisition. The emission ($^1O_2$ phosphorescence) was parked at 1270 nm with a bandpass of 30 nm. The excitation was scanned from 700 to 200 nm (i.e., to minimize photodegradation history) with a bandpass of 5 nm. Data interval and detector integration time were set to 2 nm and 0.5 s, respectively. A longer integration time would have yielded a better signal-to-noise, but we comprised it to keep photodegradation limited. To estimate the amount of photodegradation in a scan, we acquired subsequent scans (Figure 3.3), indicating 7.4% photodegradation per scan (calculation based on the maximum phosphorescence counts in each scan).

3.9.2. Excitation spectroscopy for photooxidation

Photooxidation (photodecay) rate of C_{60}, k_{pd}, was measured as a function of excitation wavelength using the Fluorolog-3 spectrofluorometer. In a typical acquisition, 100 μL of C_{60} in CCl_4 solution was placed in a standard microfluorescence cuvette (Science Outlet, 10 mm optical length, 0.35 mL capacity) and excited at selected wavelengths (from 250 to 420 nm, at 10 nm intervals) using a bandpass of 5 nm. The emission ($^1O_2$ phosphorescence) was parked at 1270 nm with a bandpass of 30 nm. At each excitation wavelength, the acquisition was performed 3 times and an unexposed sample was employed at each acquisition. The time-series phosphorescence intensity was collected in-situ at every 2s with detector integration time of 2 s. Hence, the

monochromatic optical beam of the spectrometer served as a dual probe for measurement as well as exposure simultaneously. For each excitation wavelength, k_{pd} was derived from the exponential decay rate of the phosphorescence intensity, quantifying the decay rate of C_{60} concentration.

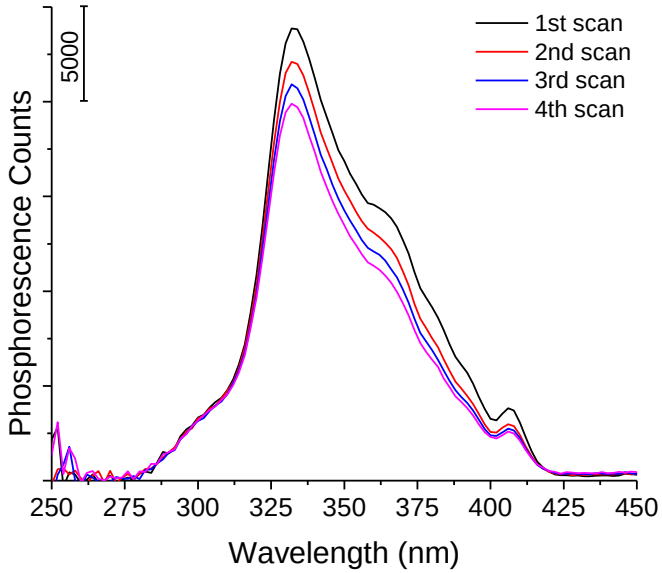

Figure 3.3: Phosphorescence (1270 nm) excitation spectra of C_{60} (in CCl_4) which were acquired in sequence.

CHAPTER IV

RESULTS AND DISCUSSION

4.1. Experimental results of C_{60} photooxidation

4.1.1. Mass spectrometry

The mass spectrum of the as-received C_{60} is shown in Figure 4.1. Only the base peak at 720 m/z was observed, confirming the high purity of C_{60} used in this work.

4.1.2. UV-Visible spectroscopy

4.1.2.1. UV exposures

Time series optical absorption spectra of C_{60} in C_6H_{14}, $CHCl_3$, and CCl_4 are shown in Figure 4.2(a-c), respectively. The major C_{60} absorption peaks at 256 and 328 nm are seen to decrease systematically, while the baseline rises indicative of a photoproduct, which is also evident from yellowing of the solution (Fig. 4.2c inset). The decay rate of C_{60} increases in solvents in the order of C_6H_{14}, $CHCl_3$, and CCl_4, which agrees with the increasing trend of the $^1O_2$ lifetime (τ) in these solvents. Figure 4.2d shows the spectrum of the excitation source which consists of a major narrow band peaking at 310 nm with no emissions below 250 nm. Hence, the possibility of O_3 generation is ruled out.[12] In Figure 4.2c, the noise below 255 nm is due to high absorption of CCl_4 attenuating the optical beam. However, it does not deteriorate the accuracy of the absorption peak of C_{60} at 260 nm (Figure 4.3).

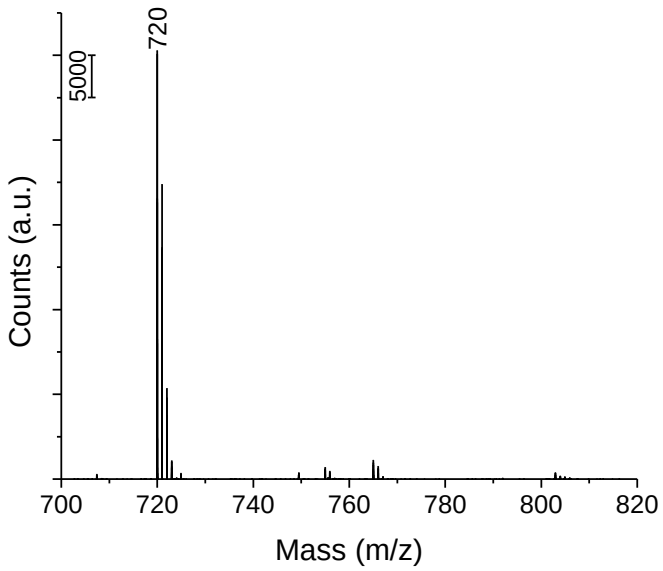

Figure 4.1: Mass spectrum of the as-received C_{60}.

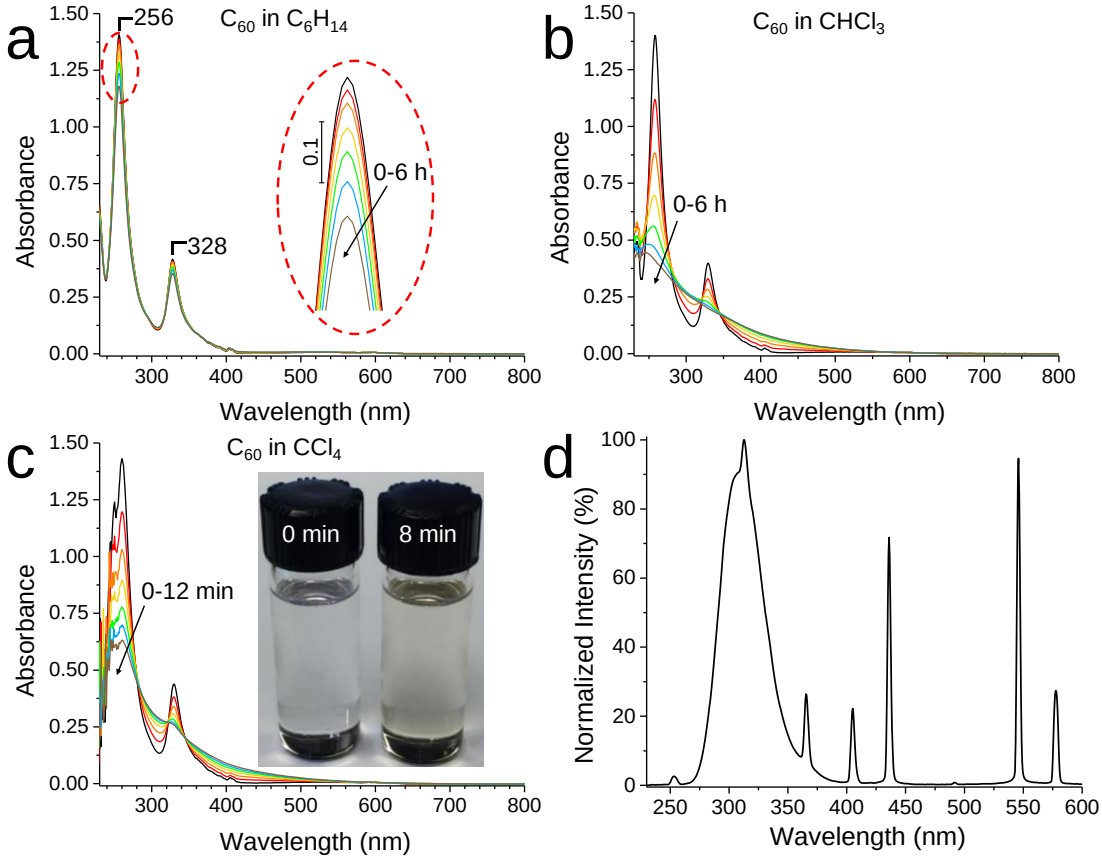

Figure 4.2: Time series absorption spectra of C_{60} in C_6H_{14} (a), $CHCl_3$ (b) and CCl_4 (c) under UV excitation of 3.74 mW/cm^2. The inset of (c) shows photos of C_{60} solutions, unexposed and after 8 min of UV exposure. (d) The spectrum of the excitation source, UVP XX-15 UV lamp.

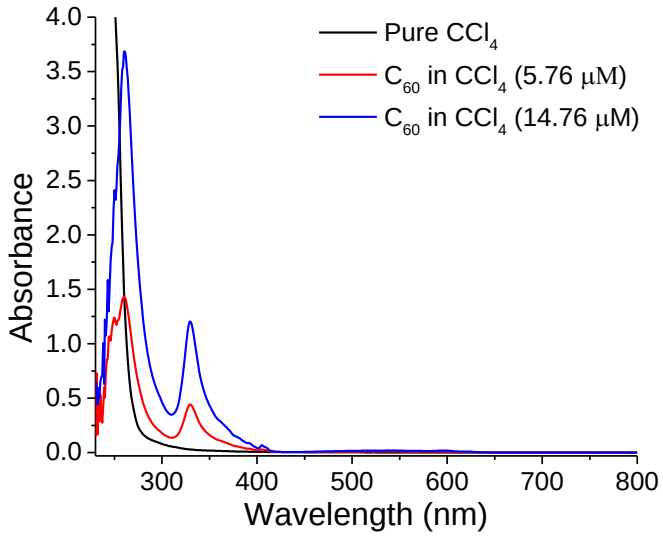

Figure 4.3: Absorption spectra of CCl_4 and C_{60} in CCl_4 at different concentrations.

As shown in Figure 4.3, the absorbance of pure CCl_4 (solvent) overwhelms absorbance of C_{60} below 260 nm. As a result, the C_{60} peak gets obscured by the solvent, especially at wavelengths below 255 nm due to the attenuation of the optical beam. To check the accuracy of our absorbance at 260 nm for the C_{60} peak, we have acquired the absorption spectrum of C_{60} at a higher concentration (i.e., 14.76 μL), so that the contribution of C_{60} is enhanced in the raw data. As seen in Figure 4.3, the C_{60} absorption peaks occur at the same wavelength for the two different concentrations. Hence, we validate the accuracy of our C_{60} absorbance values at 260 nm measured during degradation in CCl_4.

4.1.2.2. LED exposures

Time series optical absorption spectra of C_{60} in $CHCl_3$ at excitation wavelengths of 395 and 455 nm are shown in Figure 4.4. No detectable decay of C_{60} was observed after 6 h exposure. This finding agrees with the literature (Section 2.3) that PO of C_{60} cannot occur at visible (or near-visible) wavelength excitation.

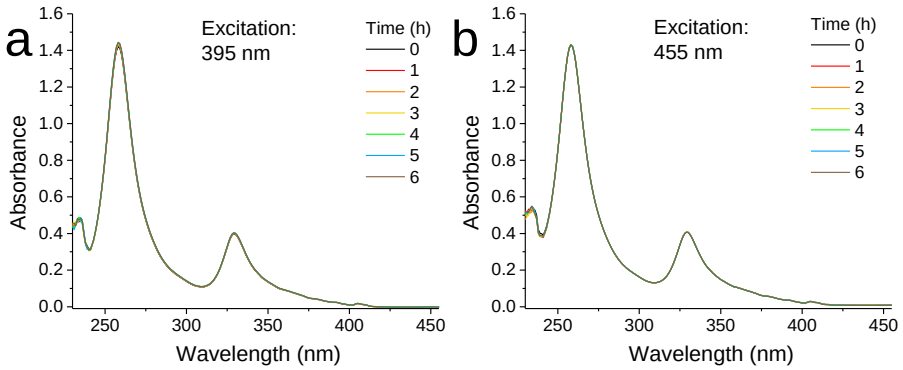

Figure 4.4: Time series absorption spectra of C_{60} (in $CHCl_3$) under 395 nm excitation of 1 mW/cm^2 (a) and 455 nm excitation of 9 mW/cm^2 (b).

4.1.3. $^1O_2$ phosphorescence by Fluorolog-3 spectrofluorometer

The phosphorescence peak at 1273 nm is shown in Figure 4.5, substantiating photosensitization of $^1O_2$ by C_{60} in the three solvents. Here, the C_{60} concentration in C_6H_{14} is 3.92 times higher than the usual concentration (i.e., 5.67 μM in Section 3.1). The intensity of phosphorescence peak increases from C_6H_{14} to CCl_4 which consists of the increasing $^1O_2$ concentration in these solvents reported in the literature. Figure 4.6 shows the $^1O_2$ phosphorescence at excitation wavelengths of 395 and 455 nm. Phosphorescence peak at 1273 nm was observed, confirming the sensitization of $^1O_2$. However, no decay of C_{60} was observed at those excitation wavelengths (Figure 4.4). It underscores the fact that sensitization of $^1O_2$ is not sufficient for the oxidation of C_{60}.

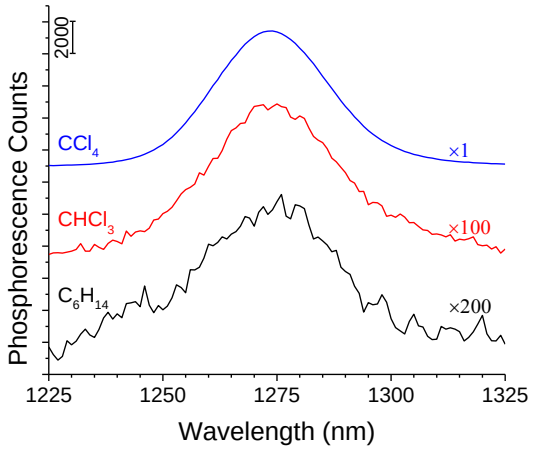

Figure 4.5: Phosphorescence spectra of $^1O_2$, sensitized by C_{60} (under 375 nm radiation of 9.5 mW/cm^2 intensity) in different solvents.

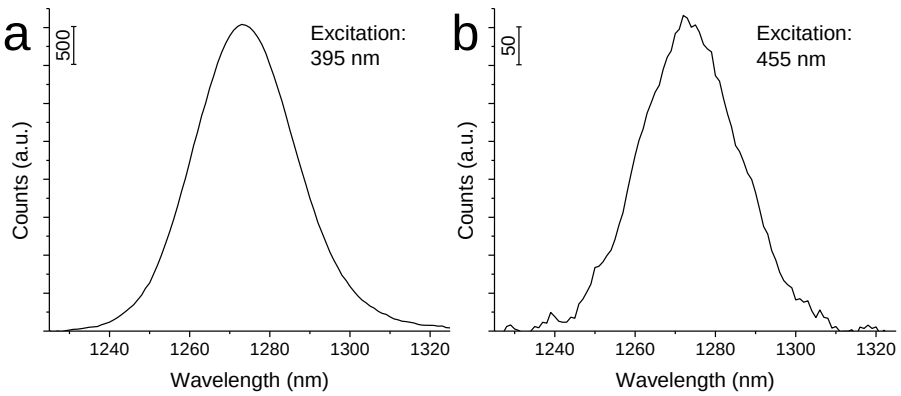

Figure 4.6: Phosphorescence spectra of $^1O_2$, sensitized by C_{60} (in CCl_4) under 395 (a) and 455 (b) nm radiation.

4.1.4. Fourier transform infrared spectroscopy

PO of C_{60} is also characterized by the FTIR spectra as shown in Figure 4.7, where C─O, C═O, and O─H stretching vibrations are indicative of C_{60} oxidation.[11] We anticipate the O─H groups result from the Norrish type II reaction.[47] The evolution of C─H vibrational peaks suggests fragmentation of the C_{60} cage subsequent to PO. The peak frequencies and important assignments are given in Figure 4.7b.[48,49] Detailed peak assignments are given in Table 4.1.

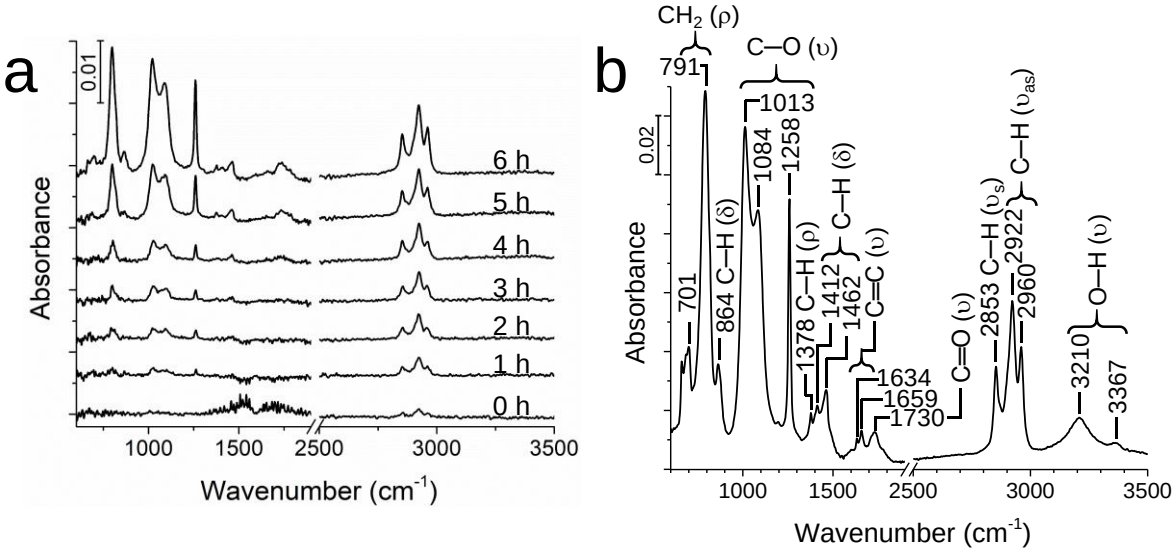

Figure 4.7: a) Time series FTIR spectra of C_{60} in $CHCl_3$ under the same UV exposure conditions as in Figure 4.2 (a-c). b) Assignment of FTIR peaks after 6 h of UV exposure (ρ: rocking; δ: bending; υ: stretching).

Table 4.1. IR mode assignments of C_{60} photoproducts after 6 h of photooxidation

Peak Position [cm^{-1}]	Assignments	Peak Position [cm^{-1}]	Assignments
701, 791	CH_2 rocking	1462	C─H scissoring
864	C─H out of plane bending	1634, 1659	C═O stretching (cyclic alkene)
1013, 1084	C─O stretching (alcohol)	1730	C═O stretching (aldehyde)
1258	C─O stretching (ether)	2853	C─H symmetric stretching (alkane)
1378	C─H rocking (methyl)	2922, 2960	C─H asymmetric stretching (alkane)
1412	C─H bending (aliphatic chain)	3210, 3367	O─H stretching (alcohol)

4.2. Kinetics analysis of C_{60} photooxidation

4.2.1. Photooxidation kinetics of C_{60} in solvents

The kinetics of C_{60}, as monitored from optical absorption, is shown in Figure 4.8. The natural logarithm of A/A_0 was plotted against exposure time (t), where A is the optical absorbance at 256 nm and A_0 is the absorbance before exposure. The graph of kinetics is linear, suggesting an exponential decay of the C_{60} population through PO, i.e., $\frac{d}{dt}[C_{60}] = -k_{pd}[C_{60}]$. The k_{pd} is the C_{60} photodecay rate, which equals to the negative slope of the straight line in the graph.

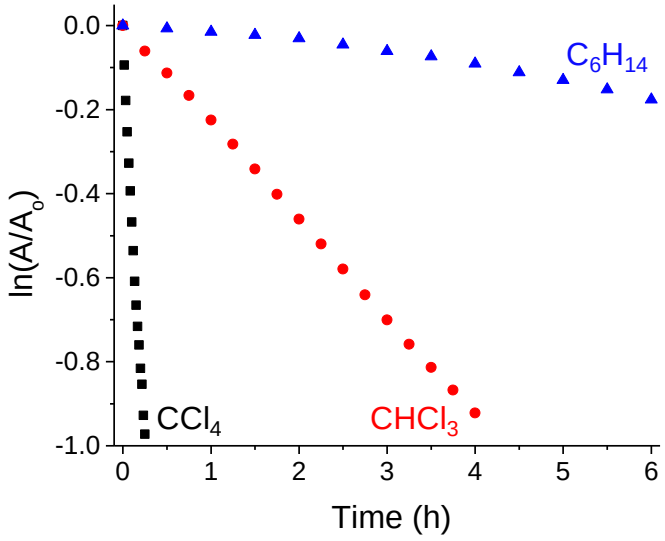

Figure 4.8: C_{60} time decay in different solvents.

4.2.2. Extraction of k_{pd} from optical absorbance of C_{60}

In this section, we validate the accuracy of k_{pd} obtained from Figure 4.8, even though the photoproduct baseline (in Figure 4.2) was not subtracted.

The oxidation kinetics (Figure 4.8), monitored from optical absorbance at 256 nm, suggest exponential decay of the C_{60} population through photooxidation. However, the time-series absorbance in Figure 4.2, $A(\mathrm{t})$, is acquired from the remaining unreacted C_{60} molecules as well as the photoproduct (i.e., oxidized/photodegraded C_{60}). Therefore,

$$A(\mathrm{t}) = A(0)e^{-k_{pd}t} + A(\infty)\left(1 - e^{-k_{pd}t}\right) \tag{4.1}$$

where $A(0)$ and $A(\infty)$ are the absorbance of the sample before any oxidation (all C_{60}) and absorbance of the photoproduct after all C_{60} reacted (all photoproduct). Here, we assume the photoproduct's chemical composition is not changing with time. This assumption is reasonable at the earlier stage of the photodegradation. Equation 4.1 may be rearranged to:

$$A(\mathrm{t}) = [A(0) - A(\infty)]e^{-k_{pd}t} + A(\infty) \tag{4.2}$$

Hence, $A(\mathrm{t})$ is an exponentially decaying function plus a constant. On the other hand, $\frac{d}{dt}A(\mathrm{t})$ is a purely an exponentially decaying function with the decay constant of k_{pd}:

$$\frac{d}{dt}A(\mathrm{t}) = -k_{pd}[A(0) - A(\infty)]e^{-k_{pd}t} \tag{4.3}$$

Therefore, k_{pd} can be derived more accurately from $\frac{d}{dt}A(\mathrm{t})$. k_{pd} is the slope of the line versus t. As an example, Figure 4.9 shows the extraction of k_{pd} for C_{60} in $CHCl_3$ from $\frac{d}{dt}A(\mathrm{t})$, where k_{pd} is found to be 6.77×10^{-5} being close to the k_{pd} value derived directly from $A(\mathrm{t})$ in Figure 4.8 (i.e., 6.47×10^{-5}). Hence, the photoproduct baseline could be ignored with negligible error and k_{pd} values derived from Figure 4.8 are reliable.

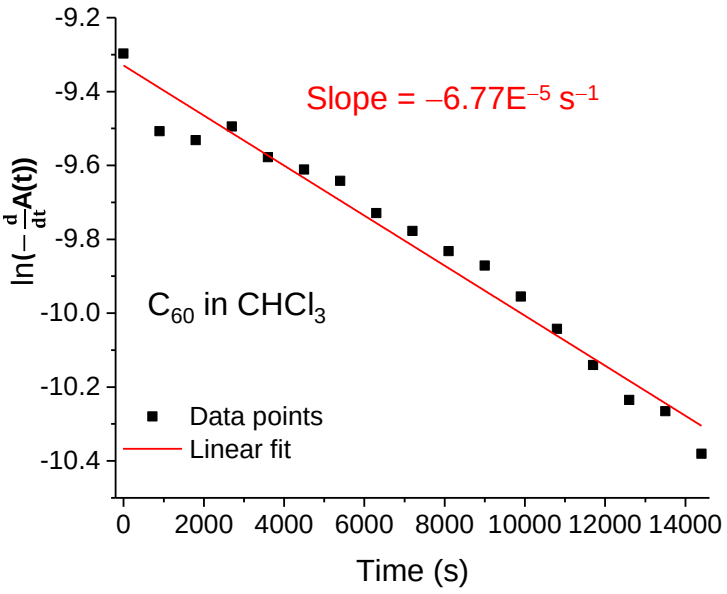

Figure 4.9: Extraction of k_{pd} from $\frac{d}{dt}A(t,\lambda)$ for C_{60} in $CHCl_3$.

4.2.3. Dependence of k_{pd} on excitation intensity

PO of C_{60} in CCl_4 at different radiation intensities (e.g., 0.62, 1.25, 2.5 and 3.74 mW/cm^2) was performed and the corresponding k_{pd} is extracted. The k_{pd} scales linearly with the radiation intensity as shown in Figure 4.10. It suggests that the PO of C_{60} is a single-photon process.

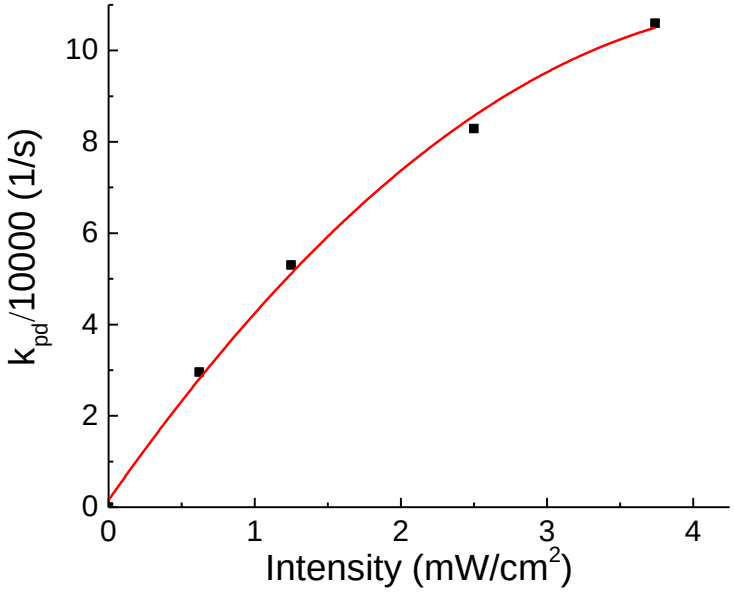

Figure 4.10: k_{pd} in CCl_4 as a function of irradiation intensity.

4.3. Mechanism of C_{60} photooxidation

4.3.1. Proposal for C_{60} photooxidation schemes

At first, we are inclined to explain the oxidation of C_{60} by its reaction with free $^1O_2$. In this model, $^1O_2$ is released to the solvent after photosensitized by a C_{60}. Subsequently, it collides and reacts with a C_{60} unless quenched by the solvent. Our mathematical analysis (Section 4.4.1) shows that this straightforward model is consistent with our observation that PO rate increases with τ. Additionally, its rate is quadratic in [C_{60}] as well as radiation intensity. On the contrary, the kinetics of C_{60}, as monitored from optical absorption (Figure 4.8) suggests exponential decay, i.e., $\frac{d}{dt}[C_{60}] = -k_{pd}[C_{60}]$, where k_{pd} is the C_{60} photodecay rate. Additionally, Figure 4.10 establishes a linear dependence of k_{pd} on excitation intensity, hence a single-photon process. Thus, we rule out 'oxidation of C_{60} with free $^1O_2$' as the dominant PO mechanism. Instead, consistent with the observed exponential decay, we propose 'oxidation with self-sensitized $^1O_2$', where a C_{60} molecule photosensitizes a $^1O_2$ and reacts with that same $^1O_2$ in a collision complex:

$$C_{60} + {}^3O_2 \xrightarrow{collision} C_{60}\bullet\ {}^3O_2 \xrightarrow{h\nu} C_{60}^*\bullet\ {}^3O_2 \xrightarrow{sensitization} C_{60}\bullet\ {}^1O_2 \xrightarrow{\text{oxidation (?)}} C_{60}O \qquad \text{(Scheme 1)}$$

Yet, Scheme 1 has a flaw with the oxidation step, where C_{60} and $^1O_2$ will not react, because C_{60} must be excited to C_{60}*. To meet this condition, a 2-photon process could be proposed, where the first photon excites C_{60} to sensitize $^1O_2$ and the second one excites C_{60} to a high energy singlet state, which thereafter reacts with $^1O_2$:

$$C_{60} + {}^3O_2 \xrightarrow{collision} C_{60}\bullet\ {}^3O_2 \xrightarrow{h\nu} C_{60}^*\bullet\ {}^3O_2 \xrightarrow{sensitization} C_{60}\bullet\ {}^1O_2 \xrightarrow{h\nu} C_{60}^*\bullet\ {}^1O_2 \xrightarrow{oxidation} C_{60}O \qquad \text{(Scheme 2)}$$

However, a two-photon process is already excluded by our results (i.e., Figure 4.10). Additionally, Scheme 2 can be ruled out by fundamental considerations. Even the longest τ (0.087 s in CCl_4) is significantly shorter than the period between two subsequent excitations of C_{60}, being 3.7 s (Section 3.5). Therefore, before the second photon absorption occurs in Scheme 2, $C_{60}\bullet{}^1O_2$ relaxes to $C_{60}\bullet{}^3O_2$ with a high probability. In other words, the excited O_2 and excited singlet C_{60} will hardly coincide in time.

Accordingly, we are urged to consider a scheme, which allows simultaneous excitation of O_2 and C_{60}, after which they coexist and react. Scheme 1 considers the most basic photosensitization event, where C_{60} returns to its ground singlet state after imparting its energy to O_2. On the other hand, it is possible that C_{60} returns to an excited singlet state, C_{60}*, (if it is photoexcited to a sufficiently high energy singlet state, C_{60}**). Accordingly, Scheme 1 may be modified to:

$$C_{60} + {}^3O_2 \xrightarrow{collision} C_{60}\bullet\ {}^3O_2 \xrightarrow{h\nu} C_{60}^{**}\bullet\ {}^3O_2 \xrightarrow{sensitization} C_{60}^{*}\bullet\ {}^1O_2 \xrightarrow{oxidation} C_{60}O \qquad \text{(Scheme 3)}$$

The lowest energy $^1C_{60}$* is 2.33 eV above the ground state. Additionally, $^1O_2$ sensitization requires 0.98 eV while 0.37 eV is lost to exchange interaction during singlet-to-triplet conversion.[28] Therefore, the minimum excitation energy of 3.68 eV is needed for Scheme 3 to succeed. Consistently, our investigation using 455 and 395 nm LED excitations (2.73 and 3.14 eV) with similar photon-count exposures as in Figure 4.2 (a-c) yielded no detectable PO (Figure 4.4), although we confirmed $^1O_2$ sensitization for these excitations from the 1273 nm phosphorescence (Figure 4.6). In Section 4.3.2, we experimentally corroborate $^1A_g \rightarrow 2^1H_u$ is the major driver of C_{60} PO in the solvents. Interestingly, $^1A_g \rightarrow 2^1H_u$ starts at 3.72 eV,[17] being very close to the threshold energy for PO (Scheme 3).

4.3.2. Validation of the proposed photooxidation schemes

4.3.2.1. Excitation spectrum for $^1O_2$ phosphorescence

Excitation spectrum for $^1O_2$ phosphorescence (sensitization) is shown in Figure 4.11a. The excitation spectrum closely follows C_{60} absorption spectrum from 700 nm down to 370 nm. This trend is consistent with constant and near-unity $^1O_2$ photosensitization quantum yield by C_{60}, Φ_S, as established in the literature.[28] The excitation spectrum below 400 nm is deconvoluted to Gaussians as shown in Figure 4.11b. Each band marks an optical transition. Although these transitions may also be resolved from optical absorption, their deconvolution is more facile from our excitation spectrum.

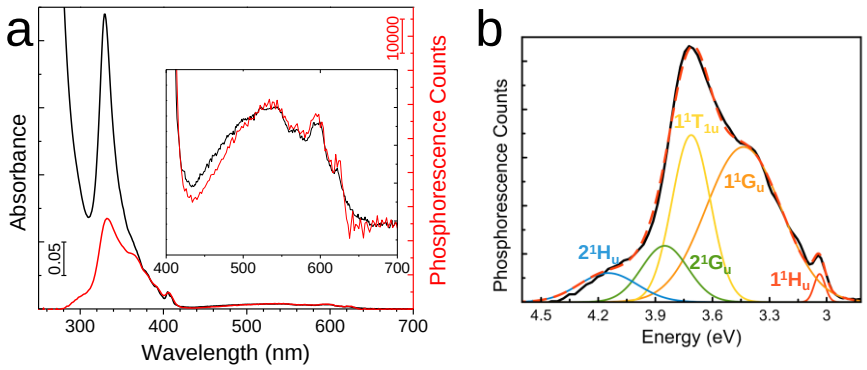

Figure 4.11: a) Overlay of absorption spectrum of C_{60} (black) and excitation spectrum for photosensitization of $^1O_2$ by C_{60}, monitored from $^1O_2$ phosphorescence counts at 1270 nm (red). b) Deconvolution of the phosphorescence excitation spectrum.

It should be mentioned that excitation spectra for phosphorescence and photosensitization of $^1O_2$ are not equivalent. However, in the present work, we consider the line shapes are the same per a given optical excitation (transition), as in the discussion of Figures 4.11. In particular, we focus on $^1A_g \longrightarrow 2\ ^1H_u$. Furthermore, we also assume the excitation line shape for photooxidation (of C_{60}) is also the same as that for phosphorescence (of $^1O_2$) per a given electronic transition. Here, we show these assumptions are exactly correct.

In excitation spectroscopy, the optical emission counts collected from a single molecule equal $I(v)\sigma_e(v)\Delta t/hv$, where I, σ_e, Δt and hv are radiation intensity, absorption cross-section for emission, signal integration time and photon energy, respectively. Using Beer-Lambert law, the counts collected from a bulk sample are $NV(I(v)\sigma_e(v)\Delta t/hv)$, where N and V are the concentration and volume of the sample. Finally, the counts are normalized by the number of incident photons per signal integration, $I(v)A\Delta t/hv$, yielding $NL\sigma_e(v)$. Here A and L are the optical beam cross-sectional area and path length (in the sample). In this analysis, I is assumed to be uniform in the sample. Hence, N should be sufficiently low or L should be sufficiently short so that the excitation beam is minimally attenuated in the sample. Otherwise, the analysis should be corrected for the decay of the beam intensity in the sample. In conclusion, the excitation spectrum for emission is $\sigma_e(v)$ multiplied by a constant.

Here, the emission is $^1O_2$ phosphorescence and $^1O_2$ belongs to the $C_{60}\bullet{}^1O_2$ complex. Additionally, $\sigma_e(v) = \sigma_s(v)\Phi_e(v)$, where σ_s is the cross-section for photosensitization of $^1O_2$ by C_{60} and $\Phi_e(v)$ is the probability of $^1O_2$ to decay (intersystem crossing to $^3O_2$) by phosphorescence. Clearly, if Φ_e has no spectral dependence (i.e., $\Phi_e(v) = constant$), then $\sigma_e(v)$ and $\sigma_s(v)$ have the same line shape. But, $\Phi_e(v) = k_e/(k_e + k_q + k_{ox}(v))$, where k's are the rate constants for $^1O_2$ emission (phosphorescence), solvent quenching (non-radiative decay) and oxidation, respectively from left to right. While k_e and k_q have no spectral dependence, k_{ox} has photon energy dependence, as our work shows. It becomes nonzero above the photon energy threshold of 3.7 eV. Nevertheless, when the excitation spectrum is deconvoluted to peaks, each peak is associated with a different optical excitation transition of C_{60}. (i.e., $S_o \longrightarrow S_n,\ n = 1,2,3, \ldots, from\ ground\ singlet\ state\ to\ excited\ n^{th}\ singlet\ state$). For a given transition (i.e., $n = 1,2,3, \ldots$), k_{ox} is independent of the photon energy, hv, because regardless of which vibronic state is excited by the photon energy, C_{60}** first relaxes vibrationally to the lowest energy vibronic state (Kasha's principle). Also, C_{60}* and $^1O_2$ after photosensitization are always the same C_{60}* and $^1O_2$ (indistinguishable of the excitation history), respectively, regardless of the photon energy for that particular optical excitation transition of C_{60} (i.e., $S_o \longrightarrow S_n,\ n = 1,2,3, \ldots$). Therefore, per a given optical excitation (transition), k_{ox} as well as Φ_e have no spectral dependence. In conclusion, $\sigma_e(v)$ and $\sigma_s(v)$ have the same line shape per a given optical excitation (e.g., $^1A_g \longrightarrow 2\ ^1H_u$). On the other hand, the overall excitation spectra for emission and sensitization (superposition of peaks associated with multiple transitions) may be different, because the ratio of cross-sections (σ_e: σ_s) may change from transition to transition (peak to peak) due to variation of k_{ox} from transition to transition (peak to peak).

Similarly, for oxidation, $\sigma_{ox}(v) = \sigma_e(v)[k_{ox}/k_e]$ from the above analysis. Hence, $\sigma_{ox}(v)$ and $\sigma_e(v)$ have the same line shape for a given excitation transition (i.e., $S_o \longrightarrow S_n,\ n = 1,2,3, \ldots$).

Thus, excitation spectra for $^1O_2$ phosphorescence and C_{60} photooxidation should have the same line shape, if they are both excited through $^1A_g \longrightarrow 2\ ^1H_u$.

4.3.2.2. Excitation spectrum for photooxidation

Excitation spectrum for oxidation (as described in Section 3.9.2) is shown in Figure 4.12. Unlike Figure 4.11a, where Φ_s diverges from the absorption spectrum and drops significantly below 370 nm. The excitation spectrum for oxidation (i.e., k_{pd}) exhibits a reverse trend. The PO rate, k_{pd}, is essentially zero for the spectral range, where Φ_s is at its maximum value of unity, but it is activated at the threshold of about 335 nm (3.7 eV), at which Φ_s is reduced to 0.37. Hence, the trends in Figure 4.11a and Figure 4.12, being spectrally different, underscore the fact that sensitization of $^1O_2$ is not sufficient for the oxidation (corroborating with Section 4.1.3). additionally, as seen in Figure 4.12, the k_{pd} spectrum matches the 2^1H_u band. These findings validate Scheme 3 as well as $^1A_g \rightarrow 2^1H_u$ being the major driver of PO. Here, the normalized k_{pd} values were derived from the $^1O_2$ phosphorescence intensity (i.e., counts proportional to $[C_{60}]$) kinetics (see Section 4.3.2.3).

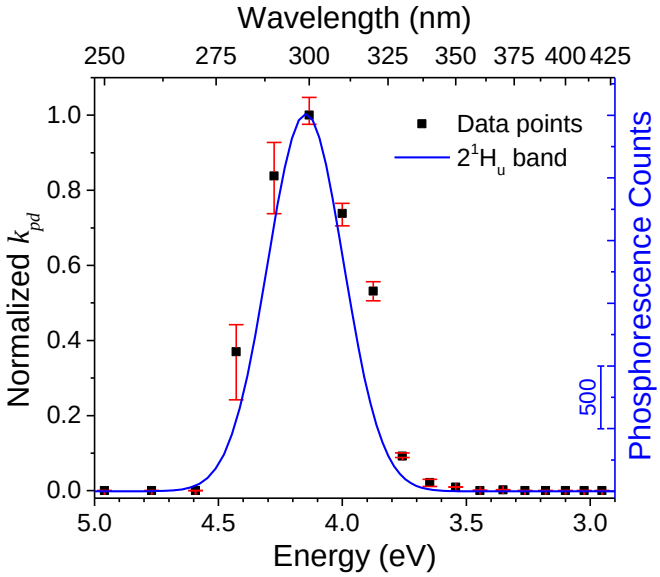

Figure 4.12: Overlay of normalized k_{pd} at different excitation wavelengths (black) and the deconvoluted 2^1H_u band (blue). Confidence interval error bars are shown (red) after 3 independent measurements.

While $1^1A_g \rightarrow 2^1H_u$ is the major driver of C_{60} PO (Scheme 3), 1^1G_u, 1^1T_{1u} and 2^1G_u states can also be excited to their vibronic levels higher than 3.7 eV (from 1^1A_g), as inferred from their deconvoluted bands in Figure 4.11b. However, vibrational relaxation (VR) is the fastest process, quickly quenching 1^1G_u, 1^1T_{1u} and 2^1G_u to their ground vibrational levels at 3.12, 3.40 and 3.43 eV, respectively. Hence, ISC from these singlet states at above 3.7 eV is expected to be outcompeted by VR. Alternatively, PO (Scheme 3) is possible from 1^1G_u, 1^1T_{1u} and 2^1G_u vibronic states, if they transition to 2^1H_u by internal conversion (IC) before VR to below 3.7 eV. Because both IC and ISC are slower than VR by an order of magnitude or more, PO from 1^1G_u, 1^1T_{1u} and 2^1G_u vibronic states will be minor, but may not be negligible. In conclusion, the major PO is expected to be through direct excitation of 2^1H_u. Accordingly, k_{pd} spectrum (data points) in Figure 4.12 follows the 2^1H_u band. However, some deviation is seen, being highest for the 3.88 eV (320 nm) data point and over the 2^1H_u Gaussian, suggestive of additional excitations contributing, possibly through 1^1G_u, 1^1T_{1u} and 2^1G_u as discussed above.

4.3.2.3. Extraction of k_{pd} from $^1O_2$ phosphorescence kinetics

Two representative plots of $^1O_2$ phosphorescence intensity kinetics are shown in Figure 4.13. These kinetics data were acquired under continuous excitation and signify decay of C_{60} by photooxidation. Figure 4.13a is representative of the kinetics we observe for excitation wavelengths between 280 to 320 nm, where the intensity of $^1O_2$ emission shows an exponential-like decay indicating loss of C_{60} to oxidation products (e.g., $C_{60}O$). On the other hand, Figure 4.13b is representative of the kinetics we observe for excitation wavelengths between 330 to 390 nm, where the emission intensity first shows an increase and then an exponential decay. Here, the monochromatic UV beam of the spectrophotometer served as excitation for both phosphorescence and photooxidation.

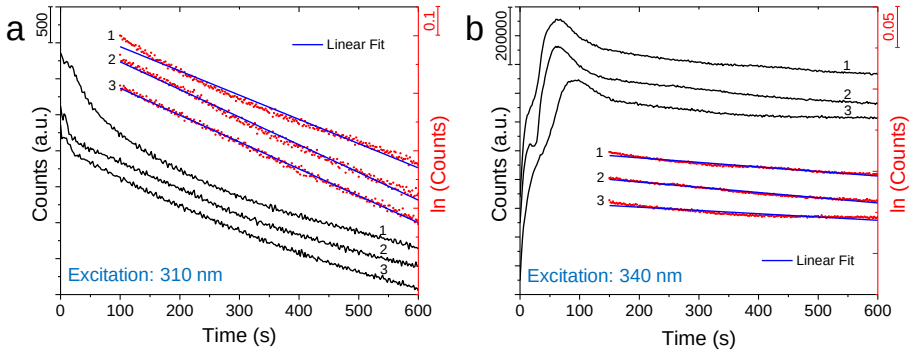

Figure 4.13: Representative plots of $^1O_2$ phosphorescence intensity kinetics under continuous excitation of 310 nm (a) and 340 nm (b) wavelength. All 3 replications are shown. The plots are intentionally offset (separated) for clarity.

The normalized k_{pd} values (by photon counts (flux)) in Figure 4.12 was derived by the following steps: 1) fitting the natural log of the $^1O_2$ phosphorescence peak intensity values (red in Figure 4.13) into a linear function (blue in Figure 4.13); 2) dividing the slope of the fitted function (blue in Figure 4.13) by the beam photon counts (flux) at the corresponding excitation wavelength (measured by the reference detector equipped in the Fluorolog; 3) normalization of the k_{pd} values by the maximum k_{pd} (occurs at 300 nm excitation).

4.4. Mathematical model of oxidation kinetics

Two mathematical models named "oxidation of C_{60} with free $^1O_2$" and "oxidation of C_{60} with self-sensitized $^1O_2$" are developed for PO of C_{60} in this work.

4.4.1. Oxidation of C_{60} with free $^1O_2$

Photooxidation of C_{60} via this scheme takes three major steps: i) photosensitization of $^1O_2$ by C_{60}; ii) accumulation of the produced $^1O_2$ in the solvent; and iii) oxidation of C_{60} after colliding with free $^1O_2$ in the solvent. In the first step, $^1O_2$ is sensitized by C_{60} as:

$$C_{60} + {}^3O_2 + h\upsilon \xrightarrow{K_s} C_{60} + {}^1O_2 \tag{4.4}$$

Here, the intermediate steps of $C_{60}\bullet{}^3O_2$ formation, photosensitization of $^1O_2$ (excitation of C_{60} to $^1C_{60}$*, intersystem crossing of $^1C_{60}$* to triplet state, $^3C_{60}$*, triplet-triplet annihilation of $^3C_{60}*\bullet{}^3O_2$ to $C_{60}\bullet{}^1O_2$) and dissociation of $C_{60}\bullet{}^1O_2$ to C_{60} and $^1O_2$ (i.e., release of $^1O_2$) are all lumped to the reaction rate constant of K_s. Hence, the generation rate of $^1O_2$ (concentration per unit time), G_s, is:

$$G_s = K_s[C_{60}]\left[\,^3O_2\right][h\upsilon] \tag{4.5}$$

where $[h\upsilon]$ stands for optical pumping rate of C_{60} being proportional to the intensity of radiation. The produced $^1O_2$ accumulates in the solvent. The decay of $^1O_2$ is mainly due to solvent quenching and the quenching rate, k_q, is the inverse of the $^1O_2$ lifetime, $k_q = 1/\tau$.

At steady state (in local time), the generation rate of $^1O_2$ is equal to its quenching rate. Therefore,

$$G_s = K_s[C_{60}][\,^3O_2][h\upsilon] = [\,^1O_2]/\tau \tag{4.6a}$$

Equation 4.6a may be rearranged to:

$$\left[\,^1O_2\right] = \tau K_s[C_{60}]\left[\,^3O_2\right][h\upsilon] \tag{4.6b}$$

The third step can occur in two ways. Either $^1O_2$ collides with an excited C_{60} and forms $^1C_{60}*\bullet{}^1O_2$, which thereafter reacts to $C_{60}O$, or it collides with ground state C_{60} forming $C_{60}\bullet{}^1O_2$, which is subsequently excited to $^1C_{60}*\bullet{}^1O_2$ and reacts. In both cases, the overall reaction is given by:

$$C_{60} + \,^1O_2 + h\upsilon \xrightarrow{K_{ox}} C_{60}O + \frac{1}{2}O_2 \tag{4.7}$$

The rate of change of C_{60} population (i.e., $\frac{d}{d_t}[C_{60}]$) follows as:

$$\frac{d}{d_t}[C_{60}] = -K_{ox}[C_{60}][\,^1O_2][h\upsilon] \tag{4.8}$$

Substituting Equation 4.6b into Equation 4.8 yields:

$$\frac{d}{d_t}[C_{60}] = -K_s K_{ox} \tau \left[{}^3O_2 \right][C_{60}]^2[h\upsilon]^2 \tag{4.9}$$

Therefore, 'oxidation of C_{60} with free $^1O_2$' is excluded as a major pathway due to the fact that Equation 4.9 is not consistent with the observed [C_{60}] kinetics, which is exponential decay. Additionally, 'oxidation of C_{60} with free $^1O_2$' is expected to have quadratic dependence on radiation intensity (i.e., two photons needed for the oxidation of a single C_{60} molecule), which is not supported by our experimental findings (i.e., Figure 4.10).

The corresponding scheme for PO of C_{60} by free $^1O_2$ is summarized as:

i) $C_{60s}\bullet\ {}^3O_2 \overset{h\upsilon}{\rightarrow} C_{60s}\bullet\ {}^1O_2 \rightarrow C_{60s} +\ {}^1O_2;\ ii)\ C_{60} \overset{h\upsilon}{\rightarrow}\ {}^1C_{60}^{*} \overset{{}^1O_2}{\longrightarrow}\ {}^1C_{60}^{*}\bullet\ {}^1O_2 \rightarrow C_{60}O$ (Scheme 4a)

i) $C_{60s}\bullet\ {}^3O_2 \overset{h\upsilon}{\rightarrow} C_{60s}\bullet\ {}^1O_2 \rightarrow C_{60s} +\ {}^1O_2; ii)\ C_{60} +\ {}^1O_2 \rightarrow C_{60}\bullet\ {}^1O_2 \overset{h\upsilon}{\rightarrow}\ {}^1C_{60}^{*}\bullet\ {}^1O_2 \rightarrow C_{60}O$ (Scheme 4b)

where C_{60s} denotes the sensitizer (photocatalyst), unlike C_{60}, which is the reactant. The overall reaction can be written as:

$$C_{60s} +\ {}^3O_2 + C_{60} + 2h\upsilon \longrightarrow C_{60}O + \frac{1}{2}O_2 + C_{60s} \tag{4.10}$$

Hence, as also seen from Equation 4.10, the forward reaction has quadratic dependence on both $[C_{60}]$ $(= [C_{60s}])$ and $[h\upsilon]$.

Additionally, 'oxidation of C_{60} with free $^1O_2$' is also ruled out as a major pathway by the following fundamental considerations. Schemes 4a and 4b are unfavorable in solvents for several reasons. First, $^1O_2$ is polar and C_{60} is highly polarizable. Hence, the release of $^1O_2$ from C_{60} is hampered in nonpolar solvents after photosensitization due to dipole – induced dipole interaction (which on the other hand benefits the 'oxidation of C_{60} by self-sensitized $^1O_2$' pathway). Second, τ is too short. As a result, the $^1O_2$ population accumulating in the solvent is limited. However, the major downfall of these Schemes is that excited C_{60} and excited O_2 are not generated

simultaneously by the same process as in our 'oxidation of C_{60} by self-sensitized $^1O_2$' scheme (Scheme 3). In Scheme 4a, the lifetime of C_{60}* is about 1 ns, while its pumping rate is 0.27 s^{-1} (Section 3.5). Hence, the concentration of C_{60}* is inferred to be negligible and its collision with a $^1O_2$ is very unlikely in such a short lifetime and low $^1O_2$ concentration. As for Scheme 4b, τ must be long enough to allow complex formation ($C_{60}\bullet{}^1O_2$) and subsequent excitation of C_{60} resulting in $C_{60}^*\bullet{}^1O_2$. The longest τ in our study (~0.1 s in CCl_4) is significantly shorter than the period between two subsequent excitations of C_{60} (~3.7 s) (Section 3.5). Hence, an excited O_2 and an excited C_{60} will hardly coincide in time and space.

On the other hand, such a condition may be allowed in a gaseous ambient by prolonged τ, which is on the order of minutes. Oxidation of C_{60} by externally generated $^1O_2$ in the gas phase and under radiation, as reported by Schuster *et al.*,[14] may, therefore, involve Scheme 4b. Interestingly, however, the excitation source employed in their work is the medium-pressure mercury lamp (200-400 nm UV radiation), which can also drive 'oxidation of C_{60} by self-sensitized $^1O_2$'.

4.4.2. Oxidation of C_{60} with self-sensitized $^1O_2$

4.4.2.1. Mathematical derivation

Figure 4.14 is a detailed mechanistic illustration of the single-photon oxidation of C_{60} with self-sensitized $^1O_2$ (Scheme 3) as unraveled in the present work. The arrows in the illustration depict the instrumental physical and chemical processes involved in Scheme 3 and are labeled with their rate constants. The initial, final and transient species involved in these processes are also shown. Among those species, 5 are included in our mathematical below. Their concentrations are denoted by c, w, x, y, z, as indicated in parentheses. Further details of Scheme 3 and its mathematical formulation are given below.

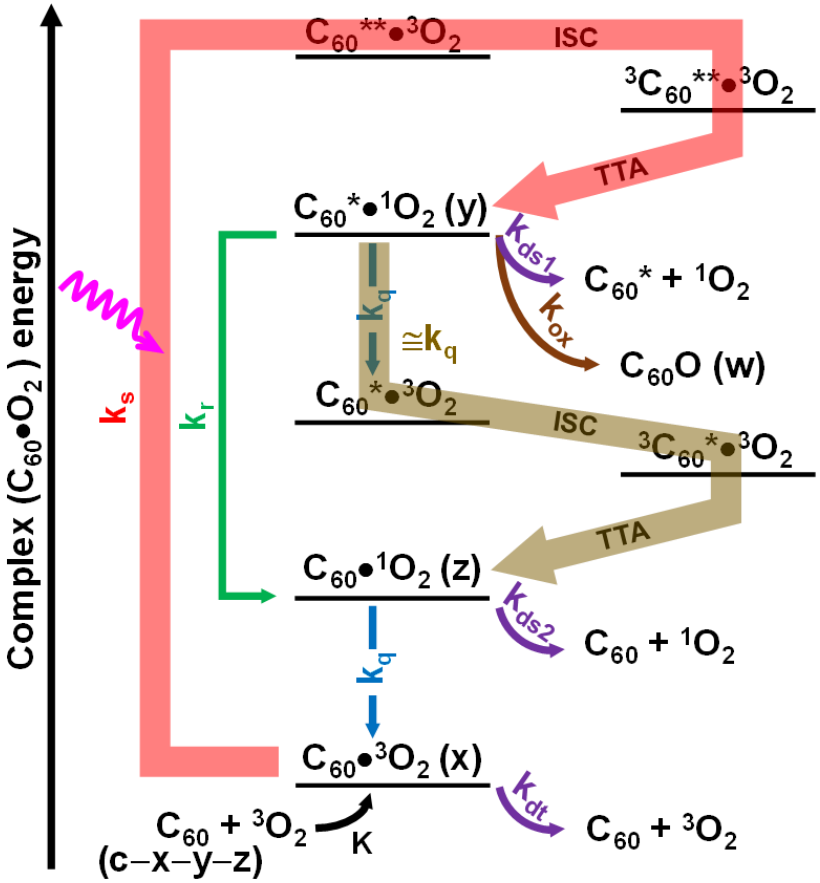

Figure 4.14: Mechanistic illustration of Scheme 3.

In the first step of Scheme 3, a collision complex, $C_{60}\bullet{}^3O_2$, forms. A ground state C_{60} collides with a ground state oxygen, ${}^3O_2$, forming a collision complex with reaction rate constant of K:

$$C_{60} + {}^3O_2 \xrightarrow{K} C_{60}\bullet\, {}^3O_2 \tag{4.11}$$

Second, C_{60} of the collision complex is photoexcited, sensitizing ${}^1O_2$ and forming ${}^1C_{60}{*}\bullet{}^1O_2$, as described by Equation 4.12. As discussed in the main text, this process actually involves the following subsequent steps: i) optical absorption, creating ${}^1C_{60}{**}\bullet{}^3O_2$; ii) intersystem crossing to ${}^3C_{60}{**}\bullet{}^3O_2$; iii) photosensitization of ${}^1O_2$ by triplet-triplet annihilation (TTA) resulting in ${}^1C_{60}{*}\bullet{}^1O_2$. The asterisks denote excited states, ** indicating the higher energy excited state. The three steps are lumped to a single rate constant of k_s. ('s' for sensitization). In terms of radiation

intensity, I, and absorption cross-section, σ_{abs}, photon energy, $h\upsilon$, and photosensitization quantum yield, Φ_s, $k_s(\upsilon) = (I(\upsilon)\sigma_{abs}(\upsilon)/h\upsilon)\Phi_s(\upsilon)$. Note that uppercase K in Equation 4.11 is the reaction rate constant, while in the remainder of this derivation we will introduce only rate constants, which are all denoted by lowercase k's.

$$C_{60}\bullet\ {}^3O_2 + h\upsilon \xrightarrow{k_s} C_{60}{}^*\bullet\ {}^1O_2 \tag{4.12}$$

Finally, C_{60} and O_2, both excited, react, as given by Equation 4.13 below. The excited complex, C_{60}*•$^1O_2$, transforms to $C_{60}O$ with a rate constant of k_{ox} ('ox' for oxidation).

$$C_{60}{}^*\bullet\ {}^1O_2 \xrightarrow{k_{ox}} C_{60}O + \frac{1}{2}O_2 \tag{4.13}$$

The rate of $C_{60}O$ formation is governed by Equation 4.14, where $\dot{w}$ is the rate of increase of $C_{60}O$ concentration; and y is the concentration of C_{60}*•$^1O_2$.

$$\dot{w} = k_{ox} \cdot y \tag{4.14}$$

C_{60}*•$^1O_2$ has four decay pathways: i) C_{60}* and $^1O_2$ react and yield $C_{60}O$ (Equation 4.13); ii) $^1O_2$ in the complex is quenched by the surrounding solvent at a quenching rate constant of k_q. Hence, C_{60}*•$^1O_2$ converts to C_{60}*•$^3O_2$. Subsequently, C_{60}*•$^3O_2$ converts to C_{60}•$^1O_2$ after intersystem crossing and TTA. The complete process may be described by: $C_{60}{}^*\bullet\ {}^1O_2 \xrightarrow{k_q} C_{60}{}^*\bullet\ {}^3O_2 \xrightarrow{ISC+TTA} C_{60}\bullet\ {}^1O_2$. Here, the second step is faster by 3 orders of magnitude or more.[28] Therefore, the decay pathway may be described shortly by: $C_{60}{}^*\bullet\ {}^1O_2 \xrightarrow{k_q} C_{60}\bullet\ {}^1O_2$; iii) C_{60}*•$^1O_2$ converts to C_{60}•$^1O_2$, where C_{60}* electronically relaxes to C_{60} with a transition rate of k_r: $C_{60}{}^*\bullet\ {}^1O_2 \xrightarrow{k_r} C_{60}\bullet\ {}^1O_2$; iv) C_{60}*•$^1O_2$ dissociates to C_{60}* and $^1O_2$ via $C_{60}{}^*\bullet\ {}^1O_2 \xrightarrow{k_{ds1}} C_{60}{}^* + {}^1O_2$ at a dissociation rate constant of k_{ds1}. Therefore, the time rate of change of C_{60}*•$^1O_2$ concentration, $\dot{y}$, is governed by:

$$\dot{y} = k_s x - k_q y - k_r y - k_{ox} y - k_{ds1} y \quad (4.15)$$

where x is the concentration of $C_{60}\bullet{}^3O_2$.

As discussed previously, $C_{60}{}^*\bullet{}^1O_2$ formation (Equation 4.12) involves the specific transition of ${}^1A_g \longrightarrow 2\ {}^1H_u$ ($C_{60} \rightarrow C_{60}{}^{**}$ *or* $C_{60}\bullet\ {}^3O_2 + h\upsilon \rightarrow C_{60}{}^{**}\bullet\ {}^3O_2$), whose theoretical photon energy threshold is 3.72 eV (experimentally, we measure the photooxidation threshold at 3.7 eV, being remarkably close to 3.72 eV, and that is how we assign the associated transition to ${}^1A_g \longrightarrow 2\ {}^1H_u$). For lower energy transitions (e.g., ${}^1A_g \longrightarrow 1\ {}^1T_{1g}$), $C_{60}\bullet{}^1O_2$ forms. Accordingly, we associate those transitions with a different sensitization rate constant, k_{s2}, (i.e., $C_{60}\bullet\ {}^3O_2 + h\upsilon \overset{k_{s2}}{\longrightarrow} C_{60}\bullet\ {}^1O_2;\ h\upsilon < 3.7\ eV$). It is possible that $C_{60}\bullet{}^1O_2$ is subsequently photoexcited with a second photon before ${}^1O_2$ is quenched and $C_{60}{}^*\bullet{}^1O_2$ forms and subsequently oxidation occurs (Equation 4.13). This oxidation pathway is represented by Scheme 2. Kinetic formulation of Scheme 2 will be provided in Section 4.4.2.4. However, the probability of this event is negligibly low if the pumping rate, k_p ($h\upsilon \geq 3.7\ eV$) or k_{p2} ($h\upsilon < 3.7\ eV$) is sufficiently lower than the ${}^1O_2$ quenching rate, k_q. As computed conservatively (overestimated but not underestimated) in Section 3.5, $k_p = 0.27\ s^{-1} \ll k_q$ in all three solvents. Additionally, we have $k_{p2} \ll k_p$, because our excitation source is limited below the photon energy of 3.7 eV (Figure 4.2d). As a result, $k_{p2} \ll k_q$ and photooxidation due to excitation of $C_{60}\bullet{}^1O_2$ is insignificant. In conclusion, we encounter insignificant 2-photon oxidation for photon energies below 3.7 eV.

Additionally, for the experimental conditions we employ in our investigation, 2-photon oxidation of C_{60} for photon energies above 3.7 eV is ignorable, too. The excitation source employed in our study is characterized by a major narrow UV band peaking at 310 nm (Figure 4.2d) which ideally favors Scheme 3. Theoretically, however, 2-photon oxidation is not impossible under this excitation. The intermediate, $C_{60}\bullet{}^1O_2$, can be excited to $C_{60}{}^{**}\bullet{}^1O_2$ (i.e., C_{60} is excited as ${}^1A_g \longrightarrow$

$2\ ^1H_u$), which is expected to undergo reaction and yield $C_{60}O$. However, for the solvents we employ, even the longest lifetime of $C_{60}\bullet{}^1O_2$ (0.087 s in CCl_4) is significantly shorter than the period between two subsequent excitations of C_{60}, being 3.7 s (Section 3.5). Therefore, we ignore 2-photon oxidation for photon energies above 3.7 eV. In conclusion, we ignore all 2-photon processes in an explanation of our experimental kinetics data.

On the other hand, the concentration of $C_{60}\bullet{}^1O_2$, z, may not be ignorable. As discussed above, $C_{60}\bullet{}^1O_2$ may be generated through the pathways: $C_{60}{}^*\bullet\ {}^1O_2 \xrightarrow{k_q} C_{60}\bullet\ {}^1O_2$ and $C_{60}{}^*\bullet\ {}^1O_2 \xrightarrow{k_r} C_{60}\bullet\ {}^1O_2$. Whereas, $C_{60}\bullet{}^1O_2$ can be quenched as: $C_{60}\bullet\ {}^1O_2 \xrightarrow{k_q} C_{60}\bullet\ {}^3O_2$. The $C_{60}\bullet{}^1O_2$ can also dissociate to C_{60} and $^1O_2$ via $C_{60}\bullet\ {}^1O_2 \xrightarrow{k_{ds2}} C_{60} +\ {}^1O_2$ at a dissociation rate constant of k_{ds2}. Accordingly, the time rate of change of z may be written as:

$$\dot{z} = (k_q + k_r)y - k_q z - k_{ds2} z \tag{4.16}$$

Note that we do not have optical excitation terms for $C_{60}\bullet{}^1O_2$, because its optical excitation is a low probability as discussed above (i.e., 2-photon processes are ignored).

As for $C_{60}\bullet{}^3O_2$, its population is determined by the following processes: i) it is generated by the collision of C_{60} and $^3O_2$ (Equation 4.11); ii) it is generated by solvent quenching of $^1O_2$ to $^3O_2$ from $C_{60}\bullet\ {}^1O_2 \xrightarrow{k_q} C_{60}\bullet\ {}^3O_2$; iii) $C_{60}\bullet{}^3O_2$ is converted to the $C_{60}{}^*\bullet{}^1O_2$ by photosensitization; iv) it dissociates to C_{60} and $^3O_2$ via reaction: $C_{60}\bullet\ {}^3O_2 \xrightarrow{k_{dt}} C_{60} +\ {}^3O_2$ with dissociation rate constant of k_{dt}. Therefore, the rate of change of $C_{60}\bullet{}^3O_2$ concentration, $\dot{x}$, is governed by:

$$\dot{x} = K[C_{60}]\left[\ {}^3O_2\right] + k_q z - k_s x - k_{dt} x \tag{4.17a}$$

Equation 4.17a may be rearranged to:

$$\dot{x} = K(c - x - y - z)\left[\ {}^3O_2\right] + k_q z - (k_s + k_{dt})x \tag{4.17b}$$

where c is the concentration of unreacted C_{60} (in complex and free forms); that is, $c = [C_{60}] + x + y + z$. The total concentration of C_{60} in all forms, reacted as well as not reacted, remains constant during the initial stage of PO, where C_{60} is intact. Hence, $c + w = constant$. Accordingly,

$$\dot{w} = -\dot{c} \tag{4.18}$$

In this kinetics model for Scheme 3, we ignore the transient populations of C_{60}*•$^3O_2$ (or C_{60}**•$^3O_2$) and $^3C_{60}$*•$^3O_2$ (or $^3C_{60}$**•$^3O_2$). C_{60}*•$^3O_2$ quickly (i.e., ~ ns; e.g., the lifetime of the S_1 state of C_{60} is 1.3 ns)[26] transforms to $^3C_{60}$*•$^3O_2$. Subsequently, $^3C_{60}$*•$^3O_2$ (or $^3C_{60}$**•$^3O_2$) rapidly (~ ns, for example, the lifetime of T_1 state of C_{60} is 330 ns in air-saturated C_6H_6)[28] undergoes TTA and converts to C_{60}*•$^1O_2$ (or C_{60}**•$^1O_2$). Hence, the accumulation of such populations is ignored.

Next, we will solve for Equations 4.15, 4.16, and 4.17b under the local steady-state approximation. This approximation holds when the rate of change of a population concentration is sufficiently lower than the number of reactions/transitions occurring per unit time per unit volume. In other words, the generation and annihilation rates approximately (but not exactly) balance each other and they are sufficiently larger than the rate of change of the population. The approximation is local in time. With this approximation, $\dot{y}$, $\dot{z}$, and $\dot{x}$ are set to 0 in Equations 4.15, 4.16 and 4.17b. Thus,

$$\dot{y} = k_s x - \left(k_q + k_r + k_{ox} + k_{ds1}\right) y = 0 \tag{4.19}$$

$$\dot{z} = (k_q + k_r) y - k_q z - k_{ds2} z = 0 \tag{4.20}$$

$$\dot{x} = K(c - x - y - z)\left[{}^3O_2\right] + k_q z - (k_s + k_{dt}) x = 0 \tag{4.21}$$

First, we solve for z and x in terms of y in Equations 4.20 and 4.21 and then substitute them in Equation 4.19 as follows:

$$z = \frac{k_q + k_r}{k_q + k_{ds2}} y$$

$$\left(k_s + k_{dt} + \mathrm{K}[\,{}^3O_2]\right)\mathrm{x} = Kc[\,{}^3O_2] + \left(\frac{k_q(k_q + k_r)}{k_q + k_{ds2}} - \mathrm{K}[\,{}^3O_2]\left(1 + \frac{k_q + k_r}{k_q + k_{ds2}}\right)\right)\mathrm{y}$$

$x = ac + by$, where $a = \frac{K[\,{}^3O_2]}{k_s + k_{dt} + \mathrm{K}[\,{}^3O_2]}$ and $\mathrm{b} = \frac{\left(\frac{k_q(k_q+k_r)}{k_q+k_{ds2}} - \mathrm{K}[\,{}^3O_2]\left(1+\frac{k_q+k_r}{k_q+k_{ds2}}\right)\right)}{k_s+k_{dt}+\mathrm{K}[\,{}^3O_2]}$

Substituting into Equation 4.19, $k_s\mathrm{ac} + k_s\mathrm{by} - \left(k_q + k_r + k_{ox} + k_{ds1}\right)\mathrm{y} = 0$. Hence,

$$y = \left(\frac{k_s a}{k_q + k_r + k_{ox} + k_{ds1} - k_s b}\right)\mathrm{c}$$

Substituting y into Equation 4.14 and combining with Equation 4.18 yields:

$$\dot{c} = -k_{ox}\mathrm{y} = -\left(\frac{k_{ox}k_s a}{k_q + k_r + k_{ox} + k_{ds1} - k_s b}\right)\mathrm{c} = -k_{pd}\mathrm{c} \qquad (4.22)$$

where $k_{pd} = \frac{k_{ox} \cdot k_s \cdot K[\,{}^3O_2]}{(k_q+k_r+k_{ox}+k_{ds1})(k_s+k_{dt}+K[\,{}^3O_2]) + k_s\left(K[\,{}^3O_2]\left(1+\frac{k_q+k_r}{k_q+k_{ds2}}\right) - \frac{k_q(k_q+k_r)}{k_q+k_{ds2}}\right)}$ is the photodecay rate constant. It is the exponential decay constant for [C_{60}].

4.4.2.2. Simplification of k_{pd} under the assumption of $[C_{60}] \ll x$ and $[C_{60}] \ll y$

Based on the literature, photosensitization of $^1O_2$ by C_{60} occurs at a quantum yield, Φ_s, of close to unity in the visible range of the electromagnetic spectrum.[26,28] Φ_s is defined as the number of $^1O_2$ sensitized divided by the number of photons absorbed by C_{60}. Hence, Φ_s being close to unity, means every photon absorption by C_{60} results in sensitization of a $^1O_2$. Accordingly, this result suggests every C_{60} must be already conjugated with a single or multiple O_2 molecule(s), unless the calculation is based on only the C_{60}, which is conjugated with $^3O_2$ (i.e. $C_{60}\bullet{}^3O_2$). However,

this detail is not provided in those references,[26,28] and the calculations quantify the concentration of C_{60} from its as-measured (i.e., total) absorption coefficient. Therefore, one may conservatively make the assumption: $[C_{60}] \ll x$ and $[C_{60}] \ll y$. This condition also implies: $k_{dt} \ll K\left[\,{}^3O_2\right]$, $k_{ds1} \ll K\left[\,{}^3O_2\right]$ and $k_{ds2} \ll K\left[\,{}^3O_2\right]$.

Under this assumption, the expression for k_{pd} above simplifies by approximation. First, from Equations 4.20 and 4.21 we have

$$K\frac{[C_{60}]}{x}\left[\,{}^3O_2\right] = (k_s + k_{dt}) - \frac{k_q(k_q+k_r)y}{(k_q+k_{ds2})x} \tag{4.23}$$

Equation 4.23 is valid for $y/x \ll 1$ as well as $y/x = 1$ (i.e., presaturation, early saturation, or saturation). Note that, saturation occurs when excessive optical pumping of C_{60} takes place to the degree that $y/x \gg 1$. Here, only k_s is directly dependent on the pumping rate. On the other hand, the rate constants k_r, k_{ds2} and k_{dt} are independent of the intensity of incident radiation to a first degree. Similarly, $K\left[\,{}^3O_2\right]$ is constant with the pumping rate to a first degree, because in the solvents we employed, $\left[\,{}^3O_2\right]/[free\ and\ conjugated\ C_{60}] > 1000$ (Section 3.2). Hence, the solvent may be treated as a reservoir of $^3O_2$. Given the assumption $[C_{60}]/x \ll 1$, then

$$K\left[\,{}^3O_2\right] \gg (k_s + k_{dt}) - \frac{k_q(k_q+k_r)y}{(k_q+k_{ds2})x} \tag{4.24}$$

For $y/x \ll 1$ (i.e., presaturation), the Inequality (4.24) suggests

$$K\left[\,{}^3O_2\right] \gg (k_s + k_{dt}) \tag{4.25}$$

For $y/x = 1$ (i.e., early saturation) the righthand side of Inequality (4.23) must still be positive. Hence, $(k_s + k_{dt}) > \frac{k_q(k_q+k_r)}{(k_q+k_{ds2})}$. Hence, from Inequality (4.25), we also infer

$$K\left[\,{}^3O_2\right] \gg \frac{k_q(k_q+k_r)}{(k_q+k_{ds2})} \text{ and } K\left[\,{}^3O_2\right]\left(1 + \frac{k_q+k_r}{k_q}\right) \gg \frac{k_q(k_q+k_r)}{(k_q+k_{ds2})} \tag{4.26}$$

Using Equation 4.25 and 4.26 as well as ignoring k_{ds1} and k_{ds2}, k_{pd} maybe approximated as:

$$k_{pd} \cong \frac{k_{ox} \cdot k_s \cdot K[\,^3O_2]}{(k_q + k_r + k_{ox})(\cong K[\,^3O_2]) + k_s(\cong K[\,^3O_2]\left(1 + \frac{k_q + k_r}{k_q}\right))} \cong \frac{k_{ox} \cdot k_s}{k_s\left(2 + \frac{k_r}{k_q}\right) + k_q + k_r + k_{ox}} \tag{4.27}$$

Indeed, the Approximation (Equation 4.27) can also be derived from Equation 4.19. Under the assumption that $[C_{60}] \ll x$, $[C_{60}] \ll y$ and $[C_{60}] \ll z$, $x + y + z \cong c$. Hence, ignoring k_{ds1} and k_{ds2} and substituting $x \cong c - y - z$ in Equation 4.19,

$$k_s(\mathrm{c} - \mathrm{y} - \frac{k_q + k_r}{k_q}\mathrm{y}) - \left(k_q + k_r + k_{ox}\right)y \cong 0$$

$$y \cong \frac{k_s}{k_s\left(2 + \frac{k_r}{k_q}\right) + k_q + k_r + k_{ox}}\, c \tag{4.28}$$

Hence, substituting Equation 4.28 in Equation 4.22, it is approximated as:

$$\dot{c} = -k_{ox}y \cong -\frac{k_{ox}k_s}{k_s\left(2 + \frac{k_r}{k_q}\right) + k_q + k_r + k_{ox}}\, c$$

from which it follows $k_{pd} \cong \frac{k_{ox} \cdot k_s}{k_s\left(2 + \frac{k_r}{k_q}\right) + k_q + k_r + k_{ox}}$, being same as Equation 4.27.

Apparently, Equation 4.27 has a singularity at $k_q = 0$, for which k_{pd} tends to zero, because of the term $k_s\left(2 + \frac{k_r}{k_q}\right)$ in the denominator tends to infinity. This situation is controversial, because k_{pd} is expected to be maximized due to an infinite lifetime of $^1O_2$. The discrepancy is due to the exclusion of two-photon processes, which is a valid assumption under the conditions employed in the current investigation as corroborated in Section 4.4.2.1 (i.e., $k_s \ll k_q$). Under this assumption, the extinction term for $C_{60}{\bullet}^1O_2$ (i.e., $[C_{60}{\bullet}^1O_2] = z$) in Equation 4.20 is only $k_q z$, once optical pumping of $C_{60}{\bullet}^1O_2$ (to $C_{60}{}^*{\bullet}^1O_2$) with a second photon is neglected. Therefore, when k_q tends to zero, there is no extinction of $C_{60}{\bullet}^1O_2$. Hence, all $C_{60}{\bullet}^3O_2$ will convert to

$C_{60}\bullet{}^1O_2$ and all $C_{60}\bullet O_2$ will accumulate in the form of $C_{60}\bullet{}^1O_2$ with an infinite lifetime of $^1O_2$. As a result, photooxidation (Scheme 3) will stop. In reality, the two-photon oxidation is non-zero and increases with decreasing k_q. Once it is included in the model, the term $k_s\left(2+\frac{k_r}{k_q}\right)$ in the denominator of Equation 4.27 will be modified to $k_s\left(2+\frac{k_r}{k_q+k_p}\right)$, where k_p is the optical pumping rate constant for $C_{60}\bullet{}^1O_2$. Hence, the singularity at $k_q = 0$ will be removed. However, there will be significant other modifications in the expression for k_{pd}, if Schemes 3 and 2 are considered in parallel.

4.4.2.3. Computation of k_r and k_{ox}

In this section, we will compute k_r and k_{ox} from the experimentally measured k_{pd} values. k_r and k_{ox} are the two unknowns in Equation 4.27 and treated as constants. k_s can be computed from the intensity of the incident radiation, the absorption coefficient of C_{60} and $^1O_2$ photosensitization quantum yield by C_{60}. We measured k_{pd} values for three solvents under the same incident excitation intensity. Therefore, k_s is also a constant. Finally, k_q is the inverse of the $^1O_2$ lifetime, τ, in the solvent and hence is the variable. Therefore, k_{pd} is a function of k_q. The two unknowns, k_r and k_{ox}, can be computed by solving two equations. Or, equivalently, they can be found as fitting parameters by fitting Equation 4.27 to the experimentally measured curve of k_{pd} versus k_q. Here, we will pursue the second strategy.

First, k_s has to be obtained. To compute k_s, $k_s = (I\sigma_{abs}/h\upsilon)\Phi_s$, we will use the excitation spectrum in the inset of Figure 4.2d. Here, the normalized spectrum, $N(\lambda)$, is for radiation intensity per wavelength, λ. Hence, the actual intensity per wavelength is $A \cdot N(\lambda)$, where A is a constant. Our UV optometer integrates radiation from 280 to 400 nm, which is $I = 3.74\ mW/cm^2$ for our PO exposures. We use this measured intensity to find A, i.e., $A\int_{280\ nm}^{400\ nm} N(\lambda)d\lambda = I = 3.74\ mW/cm^2$.

Second, we convert $A \cdot N(\lambda)$ to the function of photon energy in eV, $F(E)$. For this conversion, we have to consider the following energy balance in $d\lambda$ and dE. Also, $E = 1240/\lambda$ where E is in eV and λ is in nm.

Accordingly, $dE = -(1240/\lambda^2)d\lambda$. and $|dE| = -(1240/\lambda^2)|d\lambda|$. Therefore, $A \cdot N(\lambda)|d\lambda| = F(E)|dE| = \frac{1240 \cdot F(E)}{\lambda^2}|d\lambda|$. Hence, we write

$$F(E) = F\left(\frac{1240}{\lambda}\right) = \frac{A \cdot N(\lambda)}{1240}\lambda^2 \tag{4.29}$$

Then, k_s can be computed as:

$$k_s = \int_{3.70\ eV}^{4.43\ eV} F(E)\sigma_s(E)\frac{1}{E}dE \tag{4.30}$$

where $\sigma_s(E) = \sigma_{abs}(E)\Phi_s$ is the cross-section for photosensitization. We actually deconvoluted $\sigma_s(E)$ as a Gaussian band in Figure 4.11b and also compared it with $k_{pd}(E)$ in Figure 4.12. However, there the band was resolved from the phosphorescence excitation spectrum. The band corresponds to ${}^1A_g \longrightarrow 2\ {}^1H_u$ transition, responsible for the oxidation of C_{60}. We normalize this band to $H(E) = e^{-a(E-4.15eV)^2}$ with $a = 21.34(eV)^{-2}$. To convert $H(E)$ to $\sigma_s(E)$, we will first convert it to molar photosensitization coefficient, $\varepsilon_s(E)$, being analogous to molar attenuation coefficient, $\varepsilon(E)$. To this end, in Figure 4.11, we will compare the maximum phosphorescence counts for this band (i.e., at the peak = 299 nm), $P(299\ nm)$, with phosphorescence counts of the same curve at a different photon energy, for which ε_s is known. Conveniently, we will use the phosphorescence intensity at 406 nm, $P(406\ nm)$.

Then, $\varepsilon_s(299\ nm)/\varepsilon_s(406\ nm) = P(299\ nm)/P(406\ nm)$. However, at 406 nm, the quantum yield for photosensitization of ${}^1O_2$ by C_{60} is unity. Therefore, $\varepsilon_s(406\ nm)$, is equal to molar attenuation coefficient, $\varepsilon(406\ nm)$, which is $0.25\times10^4\ L \cdot mol^{-1} \cdot cm^{-1}$. Hence, from the well-known relation, $\sigma = 3.82 \times 10^{-21}\varepsilon$ (σ in cm^2 and ε in $L \cdot mol^{-1} \cdot cm^{-1}$), it follows:

$$\sigma_s(299\,nm) = 3.82 \times 10^{-21} \frac{P(299\,nm)}{P(406\,nm)} \varepsilon(406\,nm) = 7.14 \times 10^{-18}\,cm^2$$

Accordingly, $\sigma_s(E) = \sigma_s(299\,nm) \cdot H(E)$ and k_s now can be computed from Equation 4.30 as:

$$k_s = \sigma_s(299\,nm) \int_{3.70\,eV}^{4.43\,eV} F(E)\, e^{-21.34(eV)^{-2}(E-4.15eV)^2} \frac{1}{E} dE$$

where $F(E)$ can be fitted to a Gaussian function: $F(E) = 6.25e^{-8.75(eV)^{-2}(E-3.97eV)^2}$.

Then, k_s is computed as:

$$k_s = \sigma_s(299\,nm) \times 6.25 \int_{3.70\,eV}^{4.43\,eV} e^{-8.75(eV)^{-2}(E-3.97eV)^2}\, e^{-21.34(eV)^{-2}(E-4.15eV)^2} \frac{1}{E} dE = 0.02\ s^{-1}$$

Finally, by fitting three data points, (k_q, k_{pd}), to Equation 4.27, k_{ox} and k_r are found as 17 and 295 s^{-1}, respectively. The fitting of $k_{pd}(k_q)$ to the experimental data is shown in Figure 4.15.

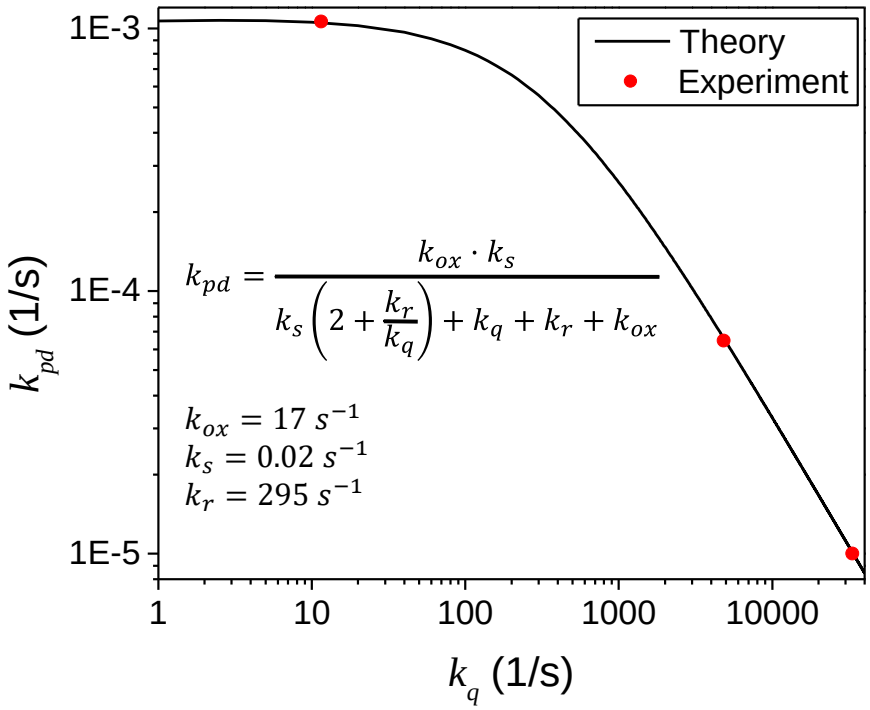

Figure 4.15: Fitting of theoretical k_{pd} expression to experimental data. The fitted values of k_{ox} and k_r are given in the inset.

4.4.2.4. Two-photon oxidation with self-sensitized C_{60} (Scheme 2)

Figure 4.16 is a detailed mechanistic illustration of the two-photon oxidation of C_{60} with self-sensitized $^1O_2$ (Scheme 2). The illustration uses the same conventions as in Figure 4.14 (Scheme 3). Making the assumptions of i) local steady-state; ii) all C_{60} is conjugated with O_2; iii) ignoring k_{ds1} and k_{ds2}, Scheme 2 may be formulated as follows:

$$\dot{y} = 0 = k_p z - (k_q + k_r + k_{ox})y \tag{4.31}$$

$$\dot{z} = 0 = k_s x + k_r y - (k_p + k_q)z \tag{4.32}$$

$$z = c - x - y \tag{4.33}$$

where k_p is the optical pumping rate constant for C_{60}.

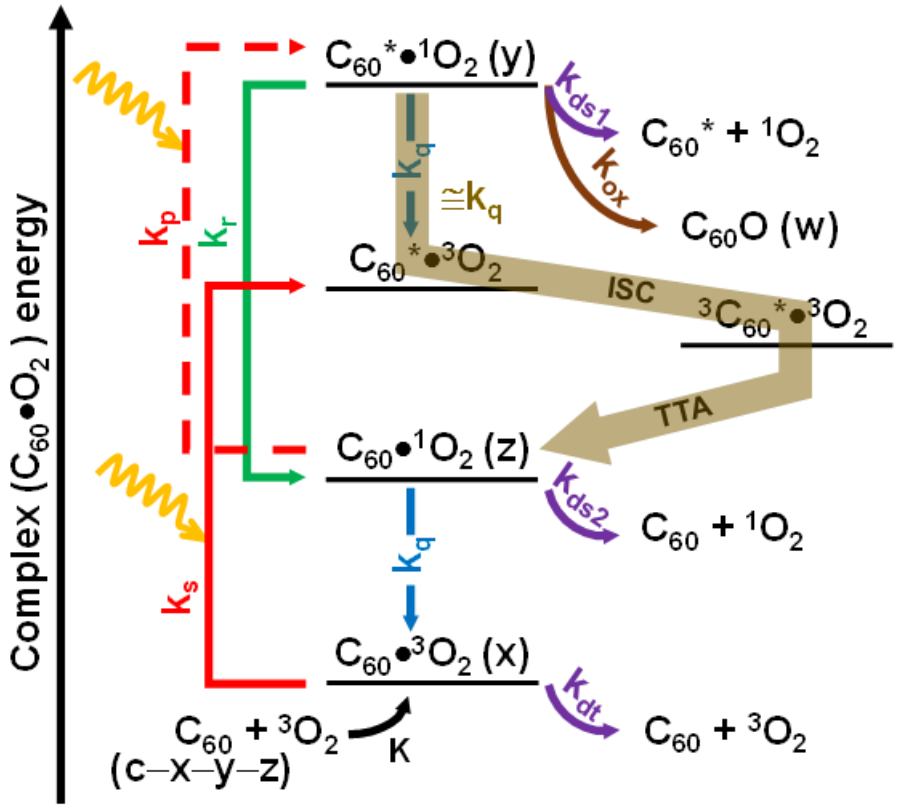

Figure 4.16: Mechanistic illustration of Scheme 2.

From Equation 4.31: $z = \frac{(k_q+k_r+k_{ox})}{k_p} y = ay$

From Equation 4.32: $x = \frac{(k_p+k_q)a - k_r}{k_s} y = by$

Substituting in Equation 4.33, $y = \frac{c}{1+a+b} = \frac{k_p k_s}{k_p k_s+(k_s+k_p+k_q)(k_q+k_r+k_{ox})-k_p k_r} c$

$$\dot{c} = -k_{ox} y = -\frac{k_{ox} k_p k_s}{k_p k_s + (k_s + k_p + k_q)(k_q + k_r + k_{ox}) - k_p k_r} c$$

In addition, remembering $k_s = k_p \Phi_s$, it follows:

$$k_{pd} = \frac{k_{ox} {k_p}^2 \Phi_s}{{k_p}^2 \Phi_s+(k_p[1+\Phi_s]+k_q)(k_q+k_r+k_{ox})-k_p k_r} \quad (4.34)$$

In our work, $k_s = 0.02\ s^{-1} \leq k_p \ll k_q$ for all three solvents studied. In this case, $k_{pd} \cong \frac{k_{ox} {k_p}^2 \Phi_s}{k_q(k_q+k_r+k_{ox})}$, having quadratic dependence on k_p. On the other hand, in air, k_q is ignorable with respect to other rate constants. Additionally, in the atmosphere, visible and UVA photons have more abundance, for which $\Phi_s \cong 1$ (i.e., $k_s \cong k_p$). Obtaining the values of k_{ox} and k_r from Section 4.2.2.3, for atmosphere:

$$k_{pd} \cong \frac{k_{ox} k_s}{k_s+k_r+2k_{ox}} = \frac{17 k_s}{k_s+329} \quad (4.35)$$

where *k* values are in 1/s.

4.4.2.5. Validation of $^1O_2$ lifetimes adopted from the literature (for the C_{60}•$^1O_2$ complex)

The $^1O_2$ lifetimes (τ) used in this work are borrowed from the literature, where $^1O_2$ was sensitized by other photosensitizers (i.e., tetraphenyl porphine, rubicene, methylene blue)[50] instead of C_{60}. In this section, using the $^1O_2$ phosphorescence peak intensities from Figure 4.5, we show those τ values are consistent and valid for C_{60}•$^1O_2$. The phosphorescence spectra of Figure 4.5 were acquired under the excitation photon energy of $h\upsilon = 3.31\ eV$.

From Section 4.4.2.1, we have $C_{60}\bullet\ ^3O_2 + h\upsilon \xrightarrow{k_{s2}} C_{60}\bullet\ ^1O_2$ for $h\upsilon < 3.7\ eV$. $^1O_2$ in the $C_{60}\bullet^1O_2$ complex is quenched by the surrounding solvent at the rate $k_q = 1/\tau$. Therefore, the time rate of change of $C_{60}\bullet^1O_2$ concentration, $\dot{z}$, is governed by:

$$\dot{z} = k_{s2}x - k_q z \tag{4.36}$$

The complex concentration, consisting of $C_{60}\bullet^3O_2$ (x) and $C_{60}\bullet^1O_2$ (z) is constant:

$$x + z = c \tag{4.37}$$

Substituting Equation 4.37 into 4.36:

$$\dot{z} = k_{s2}c - k_{s2}z - k_q z \tag{4.38}$$

Using the local steady-state approximation, $\dot{z} = 0$:

$$\mathrm{z} = \mathrm{c}\frac{k_{s2}}{k_{s2}+k_q} \tag{4.39}$$

The $^1O_2$ phosphorescence intensity is proportional to z (i.e., number of $^1O_2$ to $^3O_2$ transitions (intersystem crossing) per unit time per unit volume equals $k_{ISC}z$, where k_{ISC} is the rate constant for intersystem crossing). Hence, we write:

$$Phosphorescence\ peak\ intensity \propto z = c\frac{k_{s2}}{k_{s2}+k_q} \tag{4.40a}$$

$$Phosphorescence\ peak\ intensity = I_p(k_q) = A\frac{k_{s2}}{k_{s2}+k_q} \tag{4.40b}$$

where A is a scaling factor. k_{s2} is calculated to be 0.4 s^{-1} from Equation 3.4 using $\varepsilon = 0.6\times10^4\ M^{-1}cm^{-1}$ at $h\upsilon = 3.31$ eV. If k_q values, borrowed from the literature, are valid, then they should satisfy the relation, $I_p(k_q)$, given by Equation 4.40b. Figure 4.17 plots the measured

phosphorescence peak intensity versus quenching rate constant ($k_q = 1/\tau$). Here, values of τ for the three solvents are borrowed from Reference 41 as listed in Table 4.1.

We measured phosphorescence peak intensity for all three solvents under the same incident excitation intensity of 9.5 mW/cm^2. The sensitization rate of C_{60} is: $k_s = 0.4\ s^{-1}$. A good match is obtained between the theoretical (Equation 4.40b) trend and (k_q, I_p) data points, by fitting A to 1200000, suggesting $Intensity \propto k_s/(k_s + k_q)$. Hence, we confidently adopt the τ values from the literature.

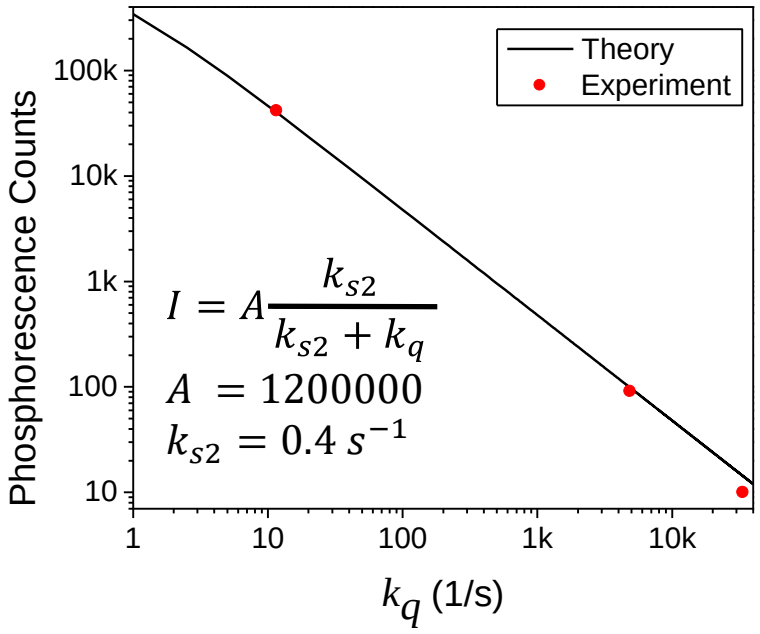

Figure 4.17: Match of theoretical $^1O_2$ phosphorescence intensity (*I*) with experiment validating the k_q values adopted from the literature. k_{s2} (0.4 s^{-1}) is the sensitization rate by C_{60}. The 2 in the subscript indicates $h\nu$ < 3.7 eV.

4.5. Photooxidation of C_{60} in atmosphere

PO of C_{60} is expected to be significantly accelerated in the atmosphere thanks to dramatically prolonged τ in the air (i.e., tens of min). Indeed, the PO can dominantly occur as a two-photon process (Scheme 2) driven by visible and UVA photons, being abundant in solar radiation. Unlike in solvents, it is challenging to monitor PO of C_{60} in air, since C_{60} being at detectable

concentrations in air, would quickly undergo aggregation as well as adsorption to enclosure walls. However, k_{pd} can be predicted from the rate constants, k_{ox} and k_r, which are already captured in the present work from C_{60} dispersions in solvents.

4.5.1. Estimation of k_{pd} in the atmosphere under solar radiation

Unlike in solvents, Scheme 2 may become significant in the atmosphere due to the longer lifetime of $^1O_2$. In this section, we validate this expectation. As discussed in the above sections, Scheme 2 can be driven by both UV and visible photons. Solar irradiation impinging on Earth is 7% UV, 47% visible, and 46% IR.[51] For simplicity, we estimate k_{pd} based on the visible irradiation only, from 400 to 700 nm. From Equation 4.30, k_s can be computed as follow:

$$k_s = \int_{1.77\ eV}^{3.10\ eV} S(E)\sigma_{abs}(E)\frac{1}{E}dE \tag{4.41}$$

where $S(E)$ is the solar irradiation as a function of photon energy in eV and $\sigma_{abs}(E)$ is the absorption cross-section of C_{60}. As in Equation 4.29, the $S(E)$ can be converted from $T(\lambda)$ as:

$$S(E) = S\left(\frac{1240}{\lambda}\right) = \frac{T(\lambda)}{1240}\lambda^2 \tag{4.42}$$

where $T(\lambda)$ is the solar intensity per wavelength, which has been provided in the literature.[52] The $\sigma_{abs}(E)$ can be computed from the well-known relation, $\sigma_{abs}(E) = 3.82 \times 10^{-21}\varepsilon(E)$, where $\varepsilon(E)$ is the molar attenuation coefficient of C_{60} as a function of photon energy in eV. We obtain $\varepsilon(E)$ from Reference 46.

To compute the integration in Equation 4.41 numerically, we fit the experimental data for $S(E)$ and $\varepsilon(E)$ into two Gaussian functions: $S(E) = 587e^{-0.58(eV)^{-2}(E-1.34)^2}$ and $\varepsilon(E) = 1022e^{-6.77(eV)^{-2}(E-2.42)^2}$. The fits are shown in Figure 4.18. Then, k_s can be computed as:

$$k_s = 3.82 \times 10^{-21}\int_{1.77eV}^{3.10\ eV} 587e^{-0.58(eV)^{-2}(E-1.34)^2} \times 1022e^{-6.77(eV)^{-2}(E-2.42)^2}\frac{1}{E}dE = 0.21\ s^{-1}$$

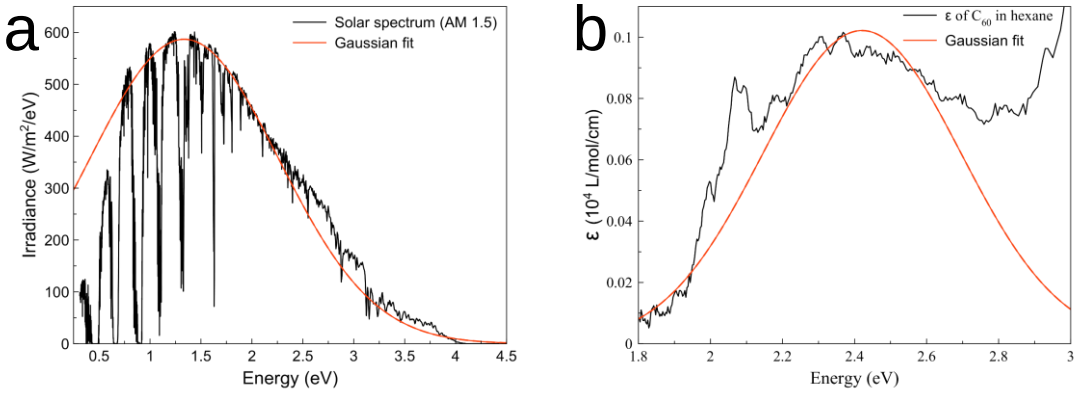

Figure 4.18: a) AM 1.5 solar irradiation as a function of photon energy. b) The molar attenuation coefficient of C_{60} in hexane. The Gaussian fit, used in the numerical integration of k_s, is shown in red.

Accordingly, k_{pd} can be computed from Equation 4.35 as:

$$k_{pd} \cong \frac{17k_s}{k_s+329} = 0.011\ s^{-1}$$

4.5.2. Half-life of C_{60} in the atmosphere

Decay of C_{60} is exponential (Figure 4.8), which can be described by Equation 4.43,

$$C_t = C_0 e^{-k_{pd}t} \tag{4.43}$$

where C_0 is the population of initial C_{60} and C_t is the remaining of C_{60} at time t. The half-life of C_{60} can be computed from Equation 4.43 by substituting $C_t = \frac{1}{2}C_0$ and $k_{pd} = 0.011\ s^{-1}$ (Section 4.5.1) as follow:

$$t = -\frac{ln\left(\frac{C_t}{C_0}\right)}{k_{pd}} = \frac{ln(2)}{k_{pd}} = 63\ s^{-1} \tag{4.44}$$

From Equation 4.44, the half-life of C_{60} is 63 s^{-1} for AM 1.5 solar radiation.

CHAPTER V

CONCLUSIONS

C_{60} has long been known to be an efficient $^1O_2$ sensitizer. Yet, no evidence has been shown that $^1O_2$ reacts with its original C_{60}, which we refer to as 'photooxidation of C_{60} with self-sensitized $^1O_2$'. This dissertation work presents strong experimental evidence for this phenomenon. In particular, we observe it as the dominant C_{60} PO mechanism in solvents. We employ a combination of the following approaches for elucidation of the phenomenon and validation of our hypotheses: PO kinetics acquisition by optical absorption spectroscopy; vibrational spectroscopy for chemical analysis; optical excitation spectroscopy; analysis of the observed kinetics through multiple models, which are mathematically developed in this work. Although the lifetime of $^1O_2$, τ, in the atmosphere is extremely long (i.e., 45 min),[40] it shortens to microseconds to nanoseconds in solvents. Inspired by this broad range of τ, we investigated PO of C_{60} in hexane (C_6H_{14}), chloroform ($CHCl_3$) and carbon tetrachloride (CCl_4), where τ is 30, 207 and 87,000 μs, respectively.[41] Our kinetics study reveals C_{60} concentration decays exponentially under UV excitation and the decay rate increases with τ. We also show the decay dominantly occurs as a single-photon process above the photon energy threshold of 3.7 eV, being the onset of $^1A_g \rightarrow 2^1H_u$ transition in C_{60}. The following conclusions are drawn:

1) PO of C_{60} by self-sensitized $^1O_2$ can occur as a single-photon process driven by the $^1A_g \rightarrow 2^1H_u$ transition with a photon energy threshold of 3.7 eV. The PO process is summarized graphically in Figure 5.1.

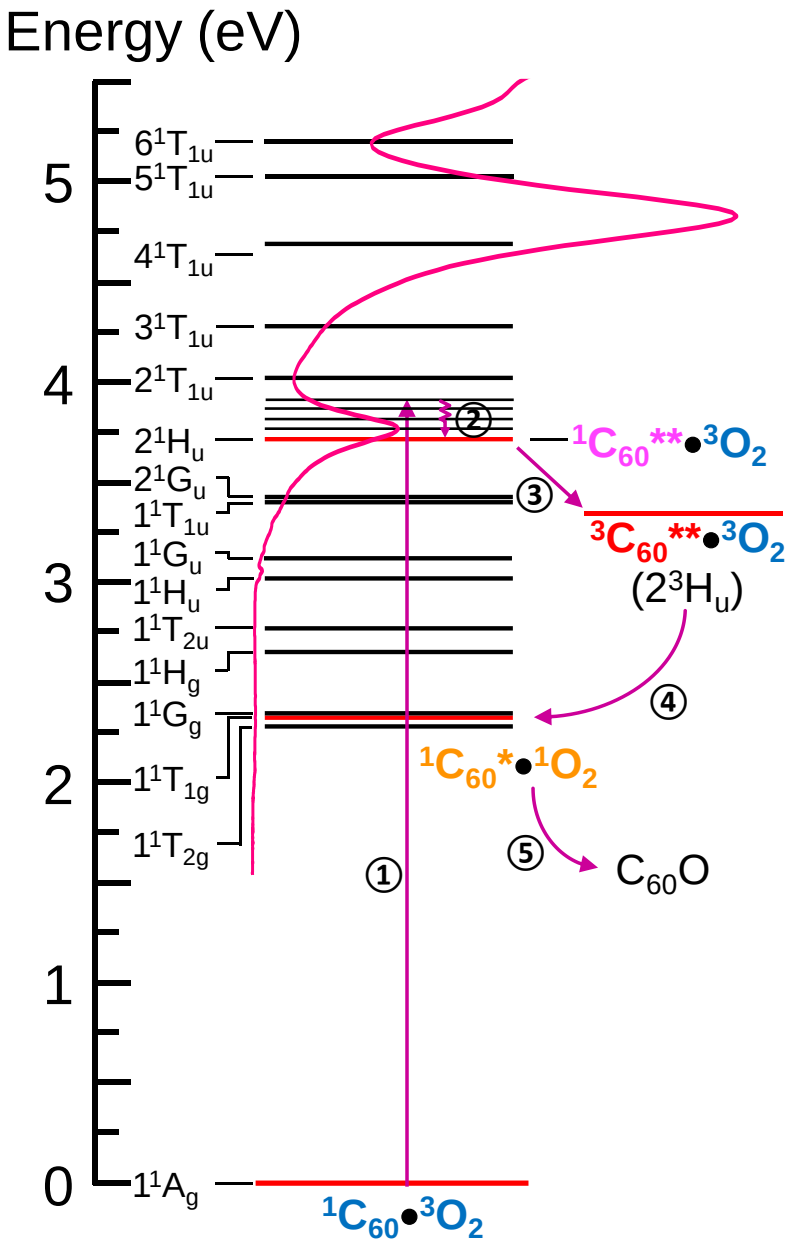

Figure 5.1: Jablonski diagram illustrating single-photon oxidation of C_{60} with self-sensitized $^1O_2$. To a first approximation, we adopt the energy structure of isolated C_{60} for the C_{60} of C_{60}•O_2. The PO process involves the following steps: ① Excitation of C_{60} to C_{60}** by a single photon which has energy equal to or higher than 3.7 eV. ② Vibrational relaxation of C_{60}**. ③ Conversion of $^1C_{60}$** to $^3C_{60}$** by ISC. ④ Sensitization of $^1O_2$ from $^3O_2$ by $^3C_{60}$** via TTA. Partial energy of $^3C_{60}$** is utilized in the $^1O_2$ sensitization, and the $^3C_{60}$** falls to a lower electronically excited state ($^1C_{60}$*). ⑤ Production of $C_{60}O$ by reaction of $^1C_{60}$* with $^1O_2$.

2) PO of C_{60} in solvents dominantly proceeds by this path; that is, self-sensitized $^1O_2$ via single-photon. The literature (prior to our work) hints both oxygen and C_{60} must be at excited states to react. This condition may immediately imply a 2-photon process, which may be explained as: oxygen is photosensitized in the first step ($^1C_{60}\bullet^1O_2$) with the first photon; then, $^1C_{60}$* is photogenerated ($^1C_{60}*\bullet^1O_2$) with the second photon. However, this scheme is not plausible in a solvent due to the limited τ. In other words, the solvent molecules would quench $^1O_2$ rapidly before the second photon is absorbed by C_{60}, as we show by computations. Additionally, intensity (radiation) dependence of the decay constant, derived in this study, corroborates a single-photon process and rules out a two-photon process.

3) However, as we validate by computations, PO of C_{60} can dominantly proceed as a two-photon process in the atmosphere thanks to dramatically prolonged τ in the air (i.e., tens of min). It can be driven by visible and UVA photons, being abundant in solar radiation. Unlike in solvents, it is challenging to monitor PO of C_{60} in air, since C_{60} being at detectable concentrations in air, would quickly undergo aggregation as well as adsorption to enclosure walls. However, k_{pd} can be predicted from the rate constants, k_{ox} and k_r, which are already captured in the present work from C_{60} dispersions in solvents. As such, we compute $k_{pd} = 0.011\ s^{-1}$ for AM 1.5 solar radiation, suggesting a half-life of 63 s. This rapid PO of C_{60} in the atmosphere potentially explains its scarceness in the environment.[53]

4) A unique triplet-triplet annihilation (TTA) process, yielding two simultaneously-excited singlets, is realized in this work, which is instrumental in PO of C_{60} with self-sensitized $^1O_2$ as a single-photon process. Specifically, $^1C_{60}*\bullet^1O_2$ is converted from $^3C_{60}**\bullet^3O_2$ by TTA. Such TTA, yielding two simultaneously-excited singlets, is different from the documented TTA in the literature which ends up with only one excited singlet. Therefore, this new scheme of TTA may empower other novel photochemistries with high efficiency.

REFERENCES

1. Kroto, H. W., Heath, J. R., O'Brien, S. C., Curl, R. F. & Smalley, R. E. C_{60}: Buckminsterfullerene. *Nature* **318**, 162–163 (1985).

2. Kratschmer, W., Lamb, L. D., Fostiropoulos, K. & Huffman, D. R. Solid C_{60}: a new form of carbon. *Nature* **347**, 354–358 (1990).

3. Hatakeyama, R., Li, Y. F., Kato, T. Y. & Kaneko, T. Infrared photovoltaic solar cells based on C_{60} fullerene encapsulated single-walled carbon nanotubes. *Appl. Phys. Lett.* **97**, 013104(1–4) (2010).

4. Vorobiev, A. K. *et al.* Fullerene as photocatalyst: Visible-light induced reaction of perfluorinated α,ω-diiodoalkanes with C_{60}. *J. Phys. Chem. A* **121**, 113–121 (2017).

5. Da Ros, T. *et al.* Synthesis and molecular modeling studies of fullerene-5,6,7-trimethoxyindole-oligonucleotide conjugates as possible probes for study of photochemical reactions in DNA triple helices. *Eur. J. Org. Chem.* **2002**, 405–413 (2002).

6. Mroz, P. *et al.* Photodynamic therapy with fullerenes. *Photochem. Photobiol. Sci.* **6**, 1139–1149 (2007).

7. Hamblin, M. R. Fullerenes as photosensitizers in photodynamic therapy: pros and cons. *Photochem. Photobiol. Sci.* **17**, 1515–1533 (2018).

8. Hou, W. & Jafvert, C. T. Photochemistry of aqueous C_{60} clusters: Evidence of $^1O_2$ formation and its role in mediating C_{60} phototransformation. *Environ. Sci. Technol.* **43**, 5257–5262 (2009).

9. Chibante, L. P. F. & Heymann, D. On the geochemistry of fullerenes: Stability of C_{60} in ambient air and the role of ozone. *Geochim. Cosmochim. Acta* **57**, 1879–1881 (1993).

10. Heymann, D. & Chibante, L. P. F. Photo-transformations of C_{60}, C_{70}, $C_{60}O$, and $C_{60}O_2$. *Chem. Phys. Lett.* **207**, 339–342 (1993).

11. Taylor, R. *et al.* Degradation of C_{60} by light. *Nature* **351**, 277 (1991).

12. Bennett, C. J. & Kaiser, R. I. Laboratory studies on the formation of ozone (O_3) on icy satellites and on interstellar and cometary ices. *Astrophys. J.* **635**, 1362–1369 (2005).

13. Taliani, C. *et al.* Light-induced oxygen incision of C_{60}. *J. Chem. Soc., Chem. Commun.* 220–222 (1993).

14. Schuster, D. I., Baran, P. S., Hatch, R. K., Khan, A. U. & Wilson, S. R. The role of singlet oxygen in the photochemical formation of $C_{60}O$. *Chem. Commun.* 2493–2494 (1998).

15. Juha, L., Hamplová, V., Kodymová, J. & Špalek, O. Reactivity of fullerenes with chemically generated singlet oxygen. *J. Chem. Soc., Chem. Commun.* 2437–2438 (1994).

16. Creegan, K. M. *et al.* Synthesis and characterization of $C_{60}O$, the first fullerene epoxide. *J. Am. Chem. Soc.* **114**, 1103–1105 (1992).

17. Negri, F., Orlandi, G. & Zerbetto, F. Interpretation of the vibrational structure of the emission and absorption spectra of C_{60}. *J. Chem. Phys.* **97**, 6496–6503 (1992).

18. Haddon, R. C., Brus, L. E. & Raghavachari, K. Electronic structure and bonding in icosahedral C_{60}. *Chem. Phys. Lett.* **125**, 459–464 (1986).

19. Orlandi, G. & Negri, F. Electronic states and transitions in C_{60} and C_{70} fullerenes. *Photochem. Photobiol. Sci.* **1**, 289–308 (2002).

20. Braga, M., Larsson, S., Rosen, A. & Volosov, A. Electronic transitions in C_{60}. On the origin of the strong interstellar absorption at 217 nm. *Astron. Astrophys.* **245**, 232–238 (1991).

21. Koeppe, R. & Sariciftci, N. S. Photoinduced charge and energy transfer involving fullerene derivatives. *Photochem. Photobiol. Sci.* **5**, 1122–1131 (2006).

22. Falke, S. M. *et al.* Coherent ultrafast charge transfer in an organic photovoltaic blend. *Science* **344**, 1001–1005 (2014).

23. Ge, Y. & Whitten, J. E. Energy level alignment between sexithiophene and buckminsterfullerene films. *Chem. Phys. Lett.* **448**, 65–69 (2007).

24. Lof, R. W., van Veenendaal, M. A., Koopmans, B., Jonkman, H. T. & Sawatzky, G. A. Band gap, excitons, and coulomb interaction in solid C_{60}. *Phys. Rev. Lett.* **68**, 3924–3927 (1992).

25. Veenstra, S. C. & Jonkman, H. T. Energy-level alignment at metal-organic and organic-organic interfaces. *J. Polym. Sci. B* **41**, 2549–2560 (2003).

26. Foote, C. S. Photophysical and Photochemical Properties of Fullerenes. in *Electron Transfer I. Topics in Current Chemistry* (ed. Mattay, J.) **169**, 348–363 (Springer-Verlag, 1994).

27. Allemand, P. M. *et al.* The unusual electron spin resonance of fullerene $C_{60}^{\bullet-}$. *J. Am. Chem. Soc.* **113**, 2780–2781 (1991).

28. Arbogast, J. W. *et al.* Photophysical properties of C_{60}. *J. Phys. Chem.* **95**, 11–12 (1991).

29. Terazima, M., Hirota, N., Shinohara, H. & Saito, Y. Photothermal investigation of the triplet state of carbon molecule C_{60}. *J. Phys. Chem.* **95**, 9080–9085 (1991).

30. Yamakoshi, Y. *et al.* Active oxygen species generated from photoexcited Fullerene (C_{60}) as Potential Medicines: $O_2^{-\bullet}$ versus $^1O_2$. *J. Am. Chem. Soc.* **125**, 12803–12809 (2003).

31. Heymann, D. *et al.* $C_{60}O_3$, a fullerene ozonide: Synthesis and dissociation to $C_{60}O$ and O_2. *J. Am. Chem. Soc.* **122**, 11473–11479 (2000).

32. Murdianti, B. S. *et al.* C_{60} oxide as a key component of aqueous C_{60} colloidal suspensions. *Environ. Sci. Technol.* **46**, 7446–7453 (2012).

33. Fortner, J. D. *et al.* Reaction of water-stable C_{60} aggregates with ozone. *Environ. Sci. Technol.* **41**, 7497–7502 (2007).

34. Wood, J. M. *et al.* Oxygen and methylene adducts of C_{60} and C_{70}. *J. Am. Chem. Soc.* **113**, 5907–5908 (1991).

35. Juha, L. *et al.* The Role of the Oxygen Molecule in the Photolysis of Fullerenes. in *Fullerene Science and Technology* **8**, 289–318 (2000).

36. Juha, L. *et al.* Fast degradation of fullerenes by ultraviolet laser radiation. *Appl. Phys. B* **B57**, 83–84 (1993).

37. Mulliken, R. S. Interpretation of the atmospheric oxygen bands; Electronic levels of the oxygen molecule. *Nature* **122**, 505 (1928).

38. Schweitzer, C. & Schmidt, R. Physical mechanisms of generation and deactivation of singlet oxygen. *Chem. Rev.* **103**, 1685–1757 (2003).

39. Kovalev, D. & Fujii, M. Silicon nanocrystals: Photosensitizers for oxygen molecules. *Adv. Mater.* **17**, 2531–2544 (2005).

40. DeRosa, M. C. & Crutchley, R. J. Photosensitized singlet oxygen and its applications. *Coord. Chem. Rev.* **233**–**234**, 351–371 (2002).

41. Turro, N. J., Ramamurthy, V. & Scaiano, J. C. Molecular Oxygen and Organic Photochemistry. in *Principles of Molecular Photochemistry: An Introduction* 1001–1042 (University Science Books, 2009).

42. Khan, A. U. & Kasha, M. Direct spectroscopic observation of singlet oxygen emission at 1268 nm excited by sensitizing dyes of biological interest in liquid solution. *Proc. Natl. Acad. Sci.* **76**, 6047–6049 (1979).

43. Battino, R. *Solubility Data Series*. *International Union of Pure and Applied Chemistry* **7**, (Pergamon Press, 1981).

44. Sato, T., Hamada, Y., Sumikawa, M., Araki, S. & Yamamoto, H. Solubility of oxygen in organic solvents and calculation of the Hansen solubility parameters of oxygen. *Ind. Eng. Chem. Res.* **53**, 19331–19337 (2014).

45. Shirono, K., Morimatsu, T. & Takemura, F. Gas solubilities (CO_2, O_2, Ar, N_2, H_2, and He) in liquid chlorinated methanes. *J. Chem. Eng. Data* **53**, 1867–1871 (2008).

46. Menéndez-Proupin, E., Delgado, A., Montero-Alejo, A. L. & García de la Vega, J. M. The absorption spectrum of C_{60} in n-hexane solution revisited: Fitted experiment and TDDFT/PCM calculations. *Chem. Phys. Lett.* **593**, 72–76 (2014).

47. Trozzolo, A. M. & Winslow, F. H. A mechanism for the oxidative photodegradation of polyethylene. *Macromolecules* **1**, 98–100 (1968).

48. Samuel, E. J. J. & Mohan, S. FTIR and FT Raman spectra and analysis of poly(4-methyl-1-pentene). *Spectrochim. Acta A* **60**, 19–24 (2004).

49. Wang, J. *et al.* Adsorption of Cu(II) on oxidized multi-walled carbon nanotubes in the presence of hydroxylated and carboxylated fullerenes. *PLoS One* **8**, e72475(1-11) (2013).

50. Schmidt, R. Influence of heavy atoms on the deactivation of singlet oxygen ($^1\Delta_g$) in solution. *J. Am. Chem. Soc.* **111**, 6983–6987 (1989).

51. Whang, A. J., Chen, Y. & Wu, B. Innovative design of cassegrain solar concentrator system for indoor illumination utilizing chromatic aberration to filter out ultraviolet and infrared in sunlight. *Sol. Energy* **83**, 1115–1122 (2009).

52. Gates, M. D. Spectral distribution of solar radiation at the earth's surface. *Science* **151**, 523–529 (1966).

53. Encinas, D. & Gómez-de-Balugera, Z. Fullerene C_{60} in atmospheric aerosol and its relationship to combustion processes. *Arch. Environ. Contam. Toxicol.* **75**, 616–624 (2018).

VITA

Linqi Zhang

Candidate for the Degree of

Doctor of Philosophy

Dissertation: SINGLE-PHOTON OXIDATION OF C_{60} BY SELF-SENSITIZED SINGLET OXYGEN

Major Field: Mechanical and Aerospace Engineering

Biographical:

Education:

Completed the requirements for the Doctor of Philosophy in Mechanical and Aerospace Engineering at Oklahoma State University, Stillwater, Oklahoma in December, 2020.

Completed the requirements for the Master of Science in Mechanical and Aerospace Engineering at Oklahoma State University, Stillwater, Oklahoma in 2014.

Completed the requirements for the Bachelor of Science in Mechanical Engineering at Harbin Institute of Technology, Harbin, China in 2012.

Experience:

Worked as a Research Associate at Oklahoma State University in Functional Nanomaterial Laboratory.